

# Modeling Dioxygen-Activating Centers in Non-Heme Diiron Enzymes: Carboxylate Shifts in Diiron(II) Complexes Supported by Sterically Hindered Carboxylate Ligands

Dongwhan Lee and Stephen J. Lippard\*

Department of Chemistry, Massachusetts Institute of Technology, Cambridge, Massachusetts 02139

Received March 8, 2002

General synthetic routes are described for a series of diiron(II) complexes supported by sterically demanding carboxylate ligands 2,6-di(*p*-tolyl)benzoate ( $\text{Ar}^{\text{ToI}}\text{CO}_2^-$ ) and 2,6-di(4-fluorophenyl)benzoate ( $\text{Ar}^{4-\text{FPh}}\text{CO}_2^-$ ). The interlocking nature of the *m*-terphenyl units in self-assembled  $[\text{Fe}_2(\mu\text{-O}_2\text{CAr}^{\text{ToI}})_2(\text{O}_2\text{CAr}^{\text{ToI}})_2\text{L}_2]$  ( $\text{L} = \text{C}_5\text{H}_5\text{N}$  (**4**); 1-Melm (**5**)) promotes the formation of coordination geometries analogous to those of the non-heme diiron cores in the enzymes RNR-R2 and  $\Delta 9\text{D}$ . Magnetic susceptibility and Mössbauer studies of **4** and **5** revealed properties consistent with weak antiferromagnetic coupling between the high-spin iron(II) centers. Structural studies of several derivatives obtained by ligand substitution reactions demonstrated that the  $[\text{Fe}_2(\text{O}_2\text{CAr}')_4\text{L}_2]$  ( $\text{Ar}' = \text{Ar}^{\text{ToI}}, \text{Ar}^{4-\text{FPh}}$ ) module is geometrically flexible. Details of ligand migration within the tetracarboxylate diiron core, facilitated by carboxylate shifts, were probed by solution variable-temperature  $^{19}\text{F}$  NMR spectroscopic studies of  $[\text{Fe}_2(\mu\text{-O}_2\text{CAr}^{4-\text{FPh}})_2(\text{O}_2\text{CAr}^{4-\text{FPh}})_2(\text{THF})_2]$  (**8**) and  $[\text{Fe}_2(\mu\text{-O}_2\text{CAr}^{4-\text{FPh}})_4(4\text{-}^i\text{BuC}_5\text{H}_4\text{N})_2]$  (**12**). Dynamic motion in the primary coordination sphere controls the positioning of open sites and regulates the access of exogenous ligands, processes that also occur in non-heme diiron enzymes during catalysis.

## Introduction

Carboxylate-bridged diiron centers are encountered at the active sites of several proteins that bind or activate dioxygen (Figure 1).<sup>1</sup> Hemerythrin (Hr) is a dioxygen-carrier protein that utilizes a ( $\mu$ -hydroxo)di( $\mu$ -carboxylato)diiron(II) core for reversible binding of dioxygen.<sup>2</sup> The hydroxylase component of soluble methane monooxygenase (MMOH),<sup>3–5</sup> the R2 component of class I ribonucleotide reductase (RNR-R2),<sup>6,7</sup>

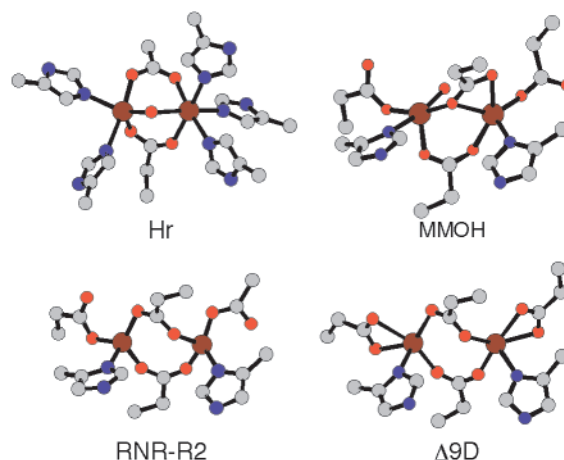


**Figure 1.** Structures of the diiron(II) centers in hemerythrin (Hr), the hydroxylase component of soluble methane monooxygenase (MMOH) from *M. capsulatus* (Bath), R2 subunit of ribonucleotide reductase (RNR-R2) from *Escherichia coli*, and stearoyl-acyl carrier protein  $\Delta^9$  desaturase ( $\Delta 9\text{D}$ ). Generated using the crystallographic coordinates.

and stearoyl-acyl carrier protein (ACP)  $\Delta^9$ -desaturase ( $\Delta 9\text{D}$ )<sup>8,9</sup> bind and redox-actively activate dioxygen. The active site

(**8**) Lindqvist, Y.; Huang, W.; Schneider, G.; Shanklin, J. *EMBO J.* **1996**, *15*, 4081–4092.

\* Author to whom correspondence should be addressed. E-mail: lippard@lippard.mit.edu.

- (1) (a) Feig, A. L.; Lippard, S. J. *Chem. Rev.* **1994**, *94*, 759–805. (b) Wallar, B. J.; Lipscomb, J. D. *Chem. Rev.* **1996**, *96*, 2625–2657. (c) Que, L., Jr.; Dong, Y. *Acc. Chem. Res.* **1996**, *29*, 190–196. (d) Lange, S. J.; Que, L., Jr. *Curr. Opin. Chem. Biol.* **1998**, *2*, 159–172. (e) Du Bois, J.; Mizoguchi, T. J.; Lippard, S. J. *Coord. Chem. Rev.* **2000**, *200–202*, 443–485. (f) Solomon, E. I.; Brunold, T. C.; Davis, M. I.; Kemsley, J. N.; Lee, S.-K.; Lehnert, N.; Neese, F.; Skulan, A. J.; Yang, Y.-S.; Zhou, J. *Chem. Rev.* **2000**, *100*, 235–349.
- (2) Stenkamp, R. E. *Chem. Rev.* **1994**, *94*, 715–726.
- (3) Valentine, A. M.; Lippard, S. J. *J. Chem. Soc., Dalton Trans.* **1997**, 3925–3931.
- (4) Whittington, D. A.; Lippard, S. J. In *Handbook of Metalloproteins*; Messerschmidt, A., Huber, R., Poulos, T., Wieghardt, K., Eds.; John Wiley & Sons: Chichester, 2001; pp 712–724.
- (5) Merckx, M.; Kopp, D. A.; Sazinsky, M. H.; Blazyk, J. L.; Müller, J.; Lippard, S. J. *Angew. Chem., Int. Ed.* **2001**, *40*, 2782–2807.
- (6) Logan, D. T.; Su, X.-D.; Åberg, A.; Regnström, K.; Hajdu, J.; Eklund, H.; Nordlund, P. *Structure* **1996**, *4*, 1053–1064.
- (7) Stubbe, J.; van der Donk, W. A. *Chem. Rev.* **1998**, *98*, 705–762.

structures of these enzymes are closely related to each other. Two bridging carboxylates support coordinatively unsaturated iron(II) centers, each having one terminal carboxylate and one histidine ligand.<sup>6,8,10</sup>

Despite the essentially identical first coordination spheres derived from the polypeptide side chains and solvent molecules in MMOH, RNR-R2, and  $\Delta 9D$ , however, the ultimate fate of dioxygen molecules that react with their diiron(II) centers is strikingly different.<sup>1</sup> MMOH catalyzes the oxidation of various organic substrates including  $\text{CH}_4$ . Formal four-electron oxidation by dioxygen affords a high-valent diiron(IV) species  $\text{Q}^{11,12}$  that inserts an  $\text{O}_2$ -derived oxygen atom into a C–H bond.<sup>5,13</sup> RNR-R2 generates a catalytically active tyrosyl radical. One-electron reduction of an initial dioxygen adduct affords a high-valent iron(III)-iron(IV) intermediate  $\text{X}$ ,<sup>14</sup> which effects the oxidation of an adjacent tyrosine residue.  $\Delta 9D$  catalyzes the insertion of a cis double bond in stearoyl-bound ACP. Although the details of the  $\Delta 9D$  reaction mechanism are less clear, a (peroxo)-diiron(III) intermediate has recently been identified,<sup>15,16</sup> which is closely related to intermediates in the MMOH and RNR-R2 reaction cycles that precede the formation of iron(IV) centers.<sup>1</sup>

The diiron(II) active sites in these functionally distinctive enzymes have attracted much attention. In parallel with direct studies of the biological systems, chemists have tried to construct and study synthetic analogues of their active sites.<sup>1c,e,17–21</sup> Such efforts have enriched our knowledge of the underlying chemical principles that govern the enzyme reaction mechanism. The quest for a unifying theory of dioxygen activation lies at the heart of such efforts, which have engendered significant advances in ligand design, synthesis, and mechanistic understanding of small molecule surrogates.

Unlike metal ions stabilized within tetrapyrrole macrocyclic ligands such as porphyrin<sup>22</sup> or corrin derivatives,<sup>23</sup> carboxylate-bridged iron(II) units are kinetically labile and

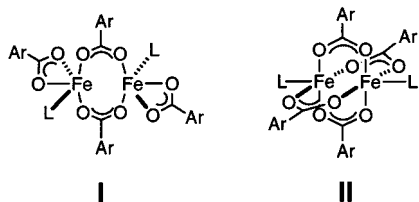
have a strong propensity to assemble into higher nuclearity species.<sup>17</sup> In the absence of a well-structured three-dimensional framework stabilizing the metal–ligand assembly, an initial and desirable kinetic product may be diverted into an unwanted thermodynamic one. Controlling the nuclearity and coordination geometry of labile metal ions on a labile ligand platform thus presents a formidable synthetic challenge. Conformationally well-defined dinucleating dicarboxylate ligands, XDK<sup>24,25</sup> and its derivatives,<sup>26,27</sup> have been extensively used in our laboratory in order to assemble coordinatively unsaturated diiron(II) complexes having the exact ligand compositions of MMOH, RNR-R2, and  $\Delta 9D$ .<sup>26,28</sup>

Despite the advances in synthetic modeling afforded by designer carboxylate ligands, however, certain limitations exist. To achieve the desired functional chemistry, the structural rigidity imparted by conformationally restrictive semi-rigid dinucleating carboxylates can be a liability. DFT calculations on MMOH indicate significant geometric rearrangement of carboxylate ligands during the reaction cycle.<sup>5,29</sup> Current information points toward trans-disposed carboxylate groups across the putative  $\{\text{Fe}_2(\mu\text{-O})_2\}^{4+}$  core in MMOH<sub>Q</sub>.<sup>12,29–31</sup> Such a structural requirement cannot be accommodated by the convergent dicarboxylate fragment in XDK, requiring a new synthetic strategy for this long-standing problem.

We previously communicated the use of a sterically demanding *m*-terphenyl-derived carboxylate ligand, 2,6-di-(*p*-tolyl)benzoate ( $\text{Ar}^{\text{ToI}}\text{CO}_2^-$ ), to reproduce key structural and functional features of the diiron(II) centers in MMOH, RNR-R2, and  $\Delta 9D$ .<sup>32,33</sup> Oxygenation of one such compound,  $[\text{Fe}_2(\mu\text{-O}_2\text{CAR}^{\text{ToI}})_2(\text{O}_2\text{CAR}^{\text{ToI}})_2(\text{N,N}\text{-Bn}_2\text{en})_2]$ ,<sup>24</sup> effected oxidative N-dealkylation of a tethered ligand fragment, further substantiating the functional relevance of the  $\text{Ar}^{\text{ToI}}\text{CO}_2^-$ -supported synthetic constructs to their C–H activating biological counterparts.<sup>34</sup> In these model compounds, interlocking tetra(carboxylate) ligand modules support either

- (9) Yang, Y.-S.; Broadwater, J. A.; Pulver, S. C.; Fox, B. G.; Solomon, E. I. *J. Am. Chem. Soc.* **1999**, *121*, 2770–2783.
- (10) (a) Rosenzweig, A. C.; Nordlund, P.; Takahara, P. M.; Frederick, C. A.; Lippard, S. J. *J. Am. Chem. Soc.* **1995**, *117*, 409–418. (b) Whittington, D. A.; Lippard, S. J. *J. Am. Chem. Soc.* **2001**, *123*, 827–838.
- (11) Liu, K. E.; Valentine, A. M.; Wang, D.; Huynh, B. H.; Edmondson, D. E.; Salifoglou, A.; Lippard, S. J. *J. Am. Chem. Soc.* **1995**, *117*, 10174–10185.
- (12) Shu, L.; Nesheim, J. C.; Kauffmann, K.; Münck, E.; Lipscomb, J. D.; Que, L., Jr. *Science* **1997**, *275*, 515–518.
- (13) Valentine, A. M.; Stahl, S. S.; Lippard, S. J. *J. Am. Chem. Soc.* **1999**, *121*, 3876–3887.
- (14) (a) Sturgeon, B. E.; Burdi, D.; Chen, S.; Huynh, B. H.; Edmondson, D. E.; Stubbe, J.; Hoffman, B. M. *J. Am. Chem. Soc.* **1996**, *118*, 7551–7557. (b) Burdi, D.; Sturgeon, B. E.; Tong, W. H.; Stubbe, J.; Hoffman, B. M. *J. Am. Chem. Soc.* **1996**, *118*, 281–282. (c) Willems, J.-P.; Lee, H.-I.; Burdi, D.; Doan, P. E.; Stubbe, J.; Hoffman, B. M. *J. Am. Chem. Soc.* **1997**, *119*, 9816–9824. (d) Burdi, D.; Willems, J.-P.; Riggs-Gelasco, P.; Antholine, W. E.; Stubbe, J.; Hoffman, B. M. *J. Am. Chem. Soc.* **1998**, *120*, 12910–12919.
- (15) Broadwater, J. A.; Ai, J.; Loehr, T. M.; Sanders-Loehr, J.; Fox, B. G. *Biochemistry* **1998**, *37*, 14664–14671.
- (16) Broadwater, J. A.; Achim, C.; Münck, E.; Fox, B. G. *Biochemistry* **1999**, *38*, 12197–12204.
- (17) Lippard, S. J. *Angew. Chem., Int. Ed. Engl.* **1988**, *27*, 344–361.
- (18) Kurtz, D. M., Jr. *Chem. Rev.* **1990**, *90*, 585–606.
- (19) Que, L., Jr. *J. Chem. Soc., Dalton Trans.* **1997**, 3933–3940.
- (20) Westerheide, L.; Pascaly, M.; Krebs, B. *Curr. Opin. Chem. Biol.* **2000**, *4*, 235–241.
- (21) Tolman, W. B.; Spencer, D. J. E. *Curr. Opin. Chem. Biol.* **2001**, *5*, 188–195.
- (22) (a) Collman, J. P.; Fu, L. *Acc. Chem. Res.* **1999**, *32*, 455–463. (b) Feiters, M. C.; Rowan, A. E.; Nolte, R. J. M. *Chem. Soc. Rev.* **2000**, *29*, 375–384. (c) Woggon, W.-D.; Wagenknecht, H.-A.; Claude, C. *J. Inorg. Biochem.* **2001**, *83*, 289–300.
- (23) (a) Pratt, J. M. *Pure Appl. Chem.* **1993**, *65*, 1513–1520. (b) Hirota, S.; Marzilli, L. G. In *Chemistry and Biochemistry of B<sub>12</sub>*; Banerjee, R., Ed.; John Wiley & Sons: New York, 1999; pp 239–260.
- (24) Abbreviations: *N,N*-Bn<sub>2</sub>en, *N,N*-dibenzylethylenediamine; TPA, tris-(2-pyridylmethyl)amine; BPMEN, *N,N'*-dimethyl-*N,N'*-bis(2-pyridylmethyl)ethylene-1,2-diamine; H<sub>2</sub>XDK, *m*-xylenediamine bis(Kemp's triacid imide).
- (25) Rebeck, J., Jr.; Marshall, L.; Wolak, R.; Parris, K.; Killoran, M.; Askew, B.; Nemeth, D.; Islam, N. *J. Am. Chem. Soc.* **1985**, *107*, 7476–7481.
- (26) Herold, S.; Lippard, S. J. *J. Am. Chem. Soc.* **1997**, *119*, 145–156.
- (27) LeCloux, D. D.; Lippard, S. J. *Inorg. Chem.* **1997**, *36*, 4035–4046.
- (28) LeCloux, D. D.; Barrios, A. M.; Mizoguchi, T. J.; Lippard, S. J. *J. Am. Chem. Soc.* **1998**, *120*, 9001–9014.
- (29) Dunitz, B. D.; Beachy, M. D.; Cao, Y.; Whittington, D. A.; Lippard, S. J.; Friesner, R. A. *J. Am. Chem. Soc.* **2000**, *122*, 2828–2839.
- (30) Siegbahn, P. E. M. *Inorg. Chem.* **1999**, *38*, 2880–2889.
- (31) Gherman, B. J.; Dunitz, B. D.; Whittington, D. A.; Lippard, S. J.; Friesner, R. A. *J. Am. Chem. Soc.* **2001**, *123*, 3836–3837.
- (32) Lee, D.; Lippard, S. J. *J. Am. Chem. Soc.* **1998**, *120*, 12153–12154.
- (33) Lee, D.; Du Bois, J.; Petasis, D.; Hendrich, M. P.; Krebs, C.; Huynh, B. H.; Lippard, S. J. *J. Am. Chem. Soc.* **1999**, *121*, 9893–9894.
- (34) (a) Lee, D.; Lippard, S. J. *J. Am. Chem. Soc.* **2001**, *123*, 4611–4612. (b) Lee, D.; Lippard, S. J. *Inorg. Chem.* **2002**, *41*, 827–837.

doubly bridged (**I**, windmill) or quadruply bridged (**II**, paddlewheel) diiron(II) cores. Low-temperature oxygenation



studies revealed the formation of high-valent Fe(III)Fe(IV) species from both **I** and **II**,<sup>33,35</sup> suggesting possible interconversion between the two isomeric forms of  $[\text{Fe}_2(\text{O}_2\text{CAR}^{\text{Tot}})_4\text{L}_2]$  ( $\text{L} = \text{N-donor ligands}$ ) in solution. In order to delineate the underlying mechanism of dioxygen activation, knowledge of the solution structure and dynamics of  $[\text{Fe}_2(\text{O}_2\text{CAR}^{\text{Tot}})_4\text{L}_2]$  is essential. In the present article we provide this information through  $^{19}\text{F}$  NMR studies of tetra(carboxylato)diiron(II) complexes having fluoro-substituted analogues of  $\text{Ar}^{\text{Tot}}\text{CO}_2^-$  as ligands. The results provide the first compelling evidence for dynamic core rearrangements via carboxylate shifts<sup>36</sup> in a  $[\text{Fe}_2(\text{O}_2\text{CR})_4\text{L}_2]$  synthetic analogue. We also describe how variations in the carboxylate and N-donor ligands can alter the geometry of these biomimetic non-heme diiron(II) compounds, the functional dioxygen-activating chemistry of which is described elsewhere.<sup>33–35</sup>

## Experimental Section

**General Considerations.** All reagents were obtained from commercial suppliers and used as received unless otherwise noted. Dichloromethane was distilled over  $\text{CaH}_2$  under nitrogen. Diethyl ether, THF, and pentanes were saturated with nitrogen and purified by passage through activated  $\text{Al}_2\text{O}_3$  columns under nitrogen.<sup>37</sup> The compounds  $\text{Fe}(\text{OTf})_2 \cdot 2\text{MeCN}$ ,<sup>38</sup>  $\text{Ar}^{\text{Tot}}\text{CO}_2\text{H}$ ,<sup>39</sup> and 2,6-di(4-fluorophenyl)benzoate ( $\text{Ar}^{4-\text{FPh}}\text{CO}_2\text{H}$ )<sup>39</sup> were prepared according to literature procedures. The sodium salts of the carboxylic acids,  $\text{NaO}_2\text{CAR}^{\text{Tot}}$  and  $\text{NaO}_2\text{CAR}^{4-\text{FPh}}$ , were prepared by treating a MeOH solution of the free acid with 1 equiv of NaOH and removing the volatile fractions under reduced pressure. Air-sensitive manipulations were carried out under nitrogen in a Vacuum Atmospheres drybox or by standard Schlenk line techniques.

**Physical Measurements.**  $^1\text{H}$  NMR and  $^{19}\text{F}$  NMR spectra were recorded on Varian Mercury 300 MHz and Inova 500 MHz spectrometers, respectively. Chemical shifts of the  $^1\text{H}$  NMR spectra are reported versus tetramethylsilane and were referenced to the residual solvent peaks.  $^{19}\text{F}$  chemical shifts are reported with reference to external  $\text{CFCl}_3$  (0.0 ppm). FT-IR spectra were recorded on a Bio Rad FTS-135 instrument with Win-IR software. UV-vis spectra were recorded on a Hewlett-Packard 8453 diode array spectrophotometer.

**$\text{TlO}_2\text{CAR}^{\text{Tot}}$ .** To a rapidly stirred THF (40 mL) solution of  $\text{Ar}^{\text{Tot}}\text{CO}_2\text{H}$  (3.00 g, 9.92 mmol) was added dropwise TlOEt (2.72

g, 10.9 mmol) diluted in THF (5 mL). The resulting white suspension was stirred for 3 h. The off-white  $\text{TlO}_2\text{CAR}^{\text{Tot}}$  solid (4.60 g, 9.10 mmol, 98%) was isolated by filtration, washed with 50 mL of THF, and dried in vacuo.  $^1\text{H}$  NMR (300 MHz, DMSO, 20 °C):  $\delta$  7.51 (d, 4H), 7.30 (t, 1H), 7.20 (t, 6H), 2.34 (s, 6H) ppm. FT-IR (KBr,  $\text{cm}^{-1}$ ): 2916, 1554, 1515, 1362, 831, 818, 798, 786, 766, 740, 702, 584, 539, 515. Anal. Calcd for  $\text{C}_{21}\text{H}_{17}\text{O}_2\text{Tl}$ : C, 49.87; H, 3.39. Found: C, 49.83; H, 3.35.

**$[\text{Fe}_2(\mu\text{-O}_2\text{CAR}^{\text{Tot}})_2(\text{THF})_2\text{Br}_2]$  (**1**) and  $[\text{Fe}_2(\mu\text{-O}_2\text{CAR}^{\text{Tot}})_2(\text{O}_2\text{CAR}^{\text{Tot}})_2(\text{THF})_2]$  (**2**).** **Method 1.** To a rapidly stirred THF solution (45 mL) of  $\text{FeBr}_2$  (397 mg, 1.84 mmol) was added  $\text{TlO}_2\text{CAR}^{\text{Tot}}$  (2.00 g, 3.95 mmol) in a single portion. The resulting heterogeneous mixture was stirred overnight (> 10 h). The suspension was filtered through Celite, and the pale yellow filtrate was concentrated under reduced pressure to give a beige solid. Vapor diffusion of pentanes into a concentrated  $\text{CH}_2\text{Cl}_2/\text{THF}$  solution of this material afforded colorless blocks of **2** (1.03 g, 0.705 mmol, 77% yield), which were suitable for X-ray crystallography. When a similar reaction was conducted for a shorter period of time (< 3 h), yellow blocks of **1** were isolated by recrystallization from  $\text{CH}_2\text{Cl}_2/\text{pentanes}$ . No further attempts were made to purify this material from  $[\text{FeBr}_2(\text{THF})_2]_n$ , a byproduct obtained as yellow blocks from the same crystallization batch.

**Method 2.** To a rapidly stirred THF (20 mL) solution of  $\text{Fe}(\text{OTf})_2 \cdot 2\text{MeCN}$  (327 mg, 0.750 mmol) was added  $\text{NaO}_2\text{CAR}^{\text{Tot}}$  (492 mg, 1.52 mmol) in a single portion. The heterogeneous mixture was stirred overnight at room temperature. Volatile fractions were removed under reduced pressure, and the residual white solid was extracted into  $\text{CH}_2\text{Cl}_2$  (10 mL). Insoluble fractions were filtered off, and the pale yellow filtrate was treated with THF (0.5 mL). Vapor diffusion of pentanes into the filtrate afforded **2** as colorless blocks (365 mg, 0.250 mmol, 67%). FT-IR (KBr,  $\text{cm}^{-1}$ ): 2918, 1605, 1543, 1515, 1456, 1410, 1384, 1187, 1110, 1037, 1020, 882, 858, 819, 801, 784, 765, 736, 714, 699, 584, 546, 539, 521. Anal. Calcd for  $\text{C}_{92}\text{H}_{84}\text{O}_{10}\text{Fe}_2$ : C, 75.62; H, 5.79. Found: C, 75.37; H, 6.03.

**$[\text{Fe}_2(\mu\text{-O}_2\text{CAR}^{\text{Tot}})_2(\text{O}_2\text{CAR}^{\text{Tot}})_2(\text{MeCN})_2]$  (**3**).** A pale yellow  $\text{CH}_2\text{Cl}_2$  (2 mL) solution of **2** (100 mg, 68.4  $\mu\text{mol}$ ) was treated with MeCN (1 mL). Vapor diffusion of pentanes into the colorless reaction mixture afforded **3** (76 mg, 54  $\mu\text{mol}$ , 79%) as colorless blocks. FT-IR (KBr,  $\text{cm}^{-1}$ ): 3051, 3021, 2918, 2862, 2307, 2281, 1589, 1541, 1515, 1456, 1412, 1384, 1307, 1213, 1186, 1149, 1110, 1073, 1033, 1020, 858, 818, 800, 790, 767, 738, 714, 702, 585, 540, 519. Anal. Calcd for  $\text{C}_{88}\text{H}_{74}\text{N}_2\text{O}_8\text{Fe}_2$ : C, 75.54; H, 5.33; N, 2.00. Found: C, 75.21; H, 5.31; N, 1.85.

**$[\text{Fe}_2(\mu\text{-O}_2\text{CAR}^{\text{Tot}})_2(\text{O}_2\text{CAR}^{\text{Tot}})_2(\text{C}_5\text{H}_5\text{N})_2]$  (**4**).** To a rapidly stirred pale yellow  $\text{CH}_2\text{Cl}_2$  solution (15 mL) of **2** (675 mg, 0.462 mmol) was added dropwise neat pyridine (82  $\mu\text{L}$ , 1.0 mmol). The solution immediately turned intense yellow, and microcrystalline material began to precipitate within minutes. The reaction mixture was kept at  $-30$  °C overnight. Ivory microcrystals of **4** (510 mg, 0.346 mmol, 75%) were isolated by filtration, washed with pentanes, and dried in vacuo. Colorless blocks suitable for X-ray crystallography were obtained by vapor diffusion of pentanes into a saturated  $\text{CH}_2\text{Cl}_2$  solution of this material at room temperature. FT-IR (KBr,  $\text{cm}^{-1}$ ): 2918, 1605, 1554, 1515, 1489, 1457, 1447, 1408, 1383, 1189, 1112, 1070, 1041, 857, 817, 802, 785, 764, 758, 736, 714, 696, 584, 545, 522. UV-vis ( $\text{CH}_2\text{Cl}_2$ ,  $\lambda_{\text{max}}$ , nm ( $\epsilon$ ,  $\text{M}^{-1}\text{cm}^{-1}$ ): 375 (1100). Anal. Calcd for  $\text{C}_{94}\text{H}_{78}\text{N}_2\text{O}_8\text{Fe}_2$ : C, 76.53; H, 5.33; N, 1.90. Found: C, 76.18; H, 5.21; N, 1.93.

**$[\text{Fe}_2(\mu\text{-O}_2\text{CAR}^{\text{Tot}})_2(\text{O}_2\text{CAR}^{\text{Tot}})_2(1\text{-MeIm})_2]$  (**5**).** This compound was prepared from **2** (266 mg, 0.182 mmol) and 1-methylimidazole (32  $\mu\text{L}$ , 0.40 mmol) by a procedure analogous to that used to obtain

- (35) Lee, D.; Pierce, B.; Krebs, C.; Hendrich, M. P.; Huynh, B. H.; Lippard, S. J. *J. Am. Chem. Soc.* **2002**, *124*, 3993–4007.  
 (36) Rardin, R. L.; Tolman, W. B.; Lippard, S. J. *New J. Chem.* **1991**, *15*, 417–430.  
 (37) Pangborn, A. B.; Giardello, M. A.; Grubbs, R. H.; Rosen, R. K.; Timmers, F. J. *Organometallics* **1996**, *15*, 1518–1520.  
 (38) Hagen, K. S. *Inorg. Chem.* **2000**, *39*, 5867–5869.  
 (39) (a) Du, C.-J. F.; Hart, H.; Ng, K.-K. D. *J. Org. Chem.* **1986**, *51*, 3162–3165. (b) Saednya, A.; Hart, H. *Synthesis* **1996**, 1455–1458. (c) Chen, C.-T.; Siegel, J. S. *J. Am. Chem. Soc.* **1994**, *116*, 5959–5960.

4. Colorless blocks of **5** (187 mg, 0.126 mmol, 69%) precipitated upon vapor diffusion of pentanes into the reaction mixture and were analyzed by X-ray crystallography. FT-IR (KBr,  $\text{cm}^{-1}$ ): 3119, 3055, 3021, 2919, 2863, 1608, 1541, 1516, 1454, 1409, 1378, 1306, 1287, 1241, 1188, 1147, 1111, 1095, 1071, 1020, 945, 847, 819, 800, 783, 765, 736, 713, 701, 656, 615, 543, 520, 453. Anal. Calcd for  $\text{C}_{92}\text{H}_{80}\text{N}_4\text{O}_8\text{Fe}_2$ : C, 74.59; H, 5.44; N, 3.78. Found: C, 74.26; H, 5.49; N, 3.48.

**[Fe<sub>2</sub>( $\mu$ -O<sub>2</sub>CAr<sup>Tol</sup>)<sub>3</sub>(O<sub>2</sub>CAr<sup>Tol</sup>)(2,6-lutidine)] (6).** A rapidly stirred  $\text{CH}_2\text{Cl}_2$  (4 mL) solution of **2** (130 mg, 89.0  $\mu\text{mol}$ ) was treated with neat 2,6-lutidine (250  $\mu\text{L}$ , 2.15 mmol). A flash of intense yellow color appeared, which gradually faded during the addition. Vapor diffusion of  $\text{Et}_2\text{O}$  into the reaction mixture afforded **6** as an off-white solid (81 mg, 57  $\mu\text{mol}$ , 64%). Colorless blocks of **6** suitable for X-ray crystallography were obtained by vapor diffusion of  $\text{Et}_2\text{O}$  into a concentrated  $\text{CH}_2\text{Cl}_2$  solution of this material at  $-30^\circ\text{C}$ . FT-IR (KBr,  $\text{cm}^{-1}$ ): 3054, 3024, 2971, 2920, 2864, 1601, 1580, 1541, 1515, 1454, 1407, 1382, 1305, 1184, 1150, 1111, 1072, 1021, 860, 844, 834, 819, 799, 784, 709, 585, 531, 470. Anal. Calcd for  $\text{C}_{91}\text{H}_{77}\text{NO}_8\text{Fe}_2$ : C, 76.74; H, 5.45; N, 0.98. Found: C, 76.55; H, 5.95; N, 0.96.

**[Fe<sub>2</sub>( $\mu$ -O<sub>2</sub>CAr<sup>Tol</sup>)<sub>4</sub>(4-<sup>t</sup>BuC<sub>5</sub>H<sub>4</sub>N)] (7).** **Method 1.** To a rapidly stirred pale yellow  $\text{CH}_2\text{Cl}_2$  solution (5 mL) of **2** (144 mg, 99  $\mu\text{mol}$ ) was added dropwise neat 4-*tert*-butylpyridine (32  $\mu\text{L}$ , 0.22 mmol). The solution was intense greenish yellow following the addition. Greenish yellow blocks of **7** (100 mg, 63  $\mu\text{mol}$ , 64%) were obtained by vapor diffusion of  $\text{Et}_2\text{O}$  into the reaction mixture. Layering of benzene over a  $\text{CH}_2\text{Cl}_2$  solution of this material provided crystals suitable for X-ray crystallography.

**Method 2.** To a rapidly stirred THF (20 mL) suspension of  $\text{NaO}_2\text{CAr}^{\text{Tol}}$  (570 mg, 1.76 mmol) was added  $\text{Fe}(\text{OTf})_2 \cdot 2\text{MeCN}$  (385 mg, 0.883 mmol) in a single portion. The heterogeneous mixture was stirred overnight, and volatile fractions were removed under reduced pressure. The residual ivory solid was extracted into  $\text{CH}_2\text{Cl}_2$  (10 mL) and filtered. A portion of 4-*tert*-butylpyridine (130  $\mu\text{L}$ , 0.880 mmol) was added to the filtrate, and the greenish yellow solution was concentrated to ca. 3 mL. Vapor diffusion of  $\text{Et}_2\text{O}$  into the solution afforded **7** (373 mg, 0.235 mmol, 53%) as greenish yellow blocks. FT-IR (KBr,  $\text{cm}^{-1}$ ): 3051, 3020, 2965, 2919, 2866, 1614, 1585, 1514, 1502, 1438, 1422, 1404, 1384, 1304, 1273, 1185, 1150, 1109, 1072, 2029, 1021, 842, 830, 812, 786, 763, 726, 712, 706, 584, 568, 525, 458. UV-vis ( $\text{CH}_2\text{Cl}_2$ ,  $\lambda_{\text{max}}$ , nm ( $\epsilon$ ,  $\text{M}^{-1}\text{cm}^{-1}$ ): 370 (1400). Anal. Calcd for  $\text{C}_{102}\text{H}_{94}\text{N}_2\text{O}_8\text{Fe}_2$ : C, 77.17; H, 5.97; N, 1.76. Found: C, 77.31; H, 6.06; N, 1.64.

**[Fe<sub>2</sub>( $\mu$ -O<sub>2</sub>CAr<sup>FPh</sup>)<sub>2</sub>(O<sub>2</sub>CAr<sup>FPh</sup>)(THF)<sub>2</sub>] (8).** This compound was prepared from  $\text{Fe}(\text{OTf})_2 \cdot 2\text{MeCN}$  (221 mg, 0.507 mmol) and  $\text{NaO}_2\text{CAr}^{\text{FPh}}$  (375 mg, 1.13 mmol) by a procedure analogous to that used to prepare **2**. Colorless blocks of **8** (192 mg, 0.129 mmol, 51%) were obtained by recrystallization from  $\text{CH}_2\text{Cl}_2$ /pentanes/hexanes and analyzed by X-ray crystallography. FT-IR (KBr,  $\text{cm}^{-1}$ ): 3063, 2975, 2886, 1608, 1514, 1458, 1413, 1384, 1300, 1219, 1186, 1160, 1094, 1071, 1035, 1014, 938, 882, 836, 809, 792, 773, 739, 712, 700, 602, 582, 555, 531, 462. Anal. Calcd for  $\text{C}_{84}\text{H}_{60}\text{O}_{10}\text{F}_8\text{Fe}_2 \cdot 0.25\text{CH}_2\text{Cl}_2$ : C, 66.82; H, 4.03. Found: C, 66.65; H, 4.05.

**[Fe<sub>2</sub>( $\mu$ -O<sub>2</sub>CAr<sup>FPh</sup>)<sub>4</sub>(THF)<sub>2</sub>] (9).** To a rapidly stirred pale yellow  $\text{CH}_2\text{Cl}_2$  (5 mL) solution of **8** (57 mg, 38  $\mu\text{mol}$ ) was added dropwise  $[\text{Cp}_2\text{Fe}](\text{PF}_6)$  (28 mg, 84  $\mu\text{mol}$ ) suspended in  $\text{CH}_2\text{Cl}_2$  (3 mL). The dark blue-green reaction mixture was stirred at room temperature for 1.5 h. Volatile fractions were removed under reduced pressure, and the residual dark green solid was washed repeatedly with pentanes. The remaining solid material was extracted into  $\text{CH}_2\text{Cl}_2$  (4 mL) and filtered. Vapor diffusion of pentanes into the filtrate afforded **9** as pale green blocks suitable

for X-ray crystallography. No further attempts were made to purify this material, which was obtained together with purple powders.

**[Fe<sub>2</sub>( $\mu$ -O<sub>2</sub>CAr<sup>FPh</sup>)<sub>4</sub>(C<sub>5</sub>H<sub>5</sub>N)<sub>2</sub>] (10).** This compound was prepared from **8** (95 mg, 64  $\mu\text{mol}$ ) and pyridine (10  $\mu\text{L}$ , 0.12 mmol) by a procedure analogous to that used to obtain **4**. Vapor diffusion of pentanes into the reaction mixture afforded **10** (61 mg, 40  $\mu\text{mol}$ , 67%) as a yellow microcrystalline solid. Single crystals suitable for X-ray crystallography were obtained by vapor diffusion of pentanes into a saturated  $\text{CH}_2\text{Cl}_2$  solution of this material at  $-30^\circ\text{C}$ . FT-IR (KBr,  $\text{cm}^{-1}$ ): 3057, 1605, 1551, 1510, 1488, 1449, 1404, 1381, 1300, 1225, 1160, 1096, 1071, 1042, 1011, 843, 809, 792, 771, 704, 582, 555, 530, 464. UV-vis ( $\text{CH}_2\text{Cl}_2$ ,  $\lambda_{\text{max}}$ , nm ( $\epsilon$ ,  $\text{M}^{-1}\text{cm}^{-1}$ ): 366 (930). Anal. Calcd for  $\text{C}_{86}\text{H}_{54}\text{N}_2\text{O}_8\text{F}_8\text{Fe}_2$ : C, 68.54; H, 3.61; N, 1.86. Found: C, 68.49; H, 3.70; N, 1.92.

**[Fe<sub>2</sub>( $\mu$ -O<sub>2</sub>CAr<sup>FPh</sup>)<sub>4</sub>(1-MeIm)<sub>2</sub>] (11).** This compound was prepared in a manner similar to that described for **10**, except that 1-methylimidazole was used instead of pyridine. Pale yellow blocks of **11** (44%) suitable for X-ray crystallography were obtained by vapor diffusion of pentanes/hexanes (1:1) into the reaction mixture. FT-IR (KBr,  $\text{cm}^{-1}$ ): 3136, 3059, 2962, 2928, 1605, 1535, 1511, 1454, 1404, 1381, 1222, 1160, 1094, 1015, 948, 842, 809, 792, 771, 714, 705, 655, 555, 531, 466. Anal. Calcd for  $\text{C}_{84}\text{H}_{56}\text{N}_4\text{O}_8\text{F}_8\text{Fe}_2$ : C, 66.68; H, 3.73; N, 3.70. Found: C, 66.71; H, 4.03; N, 3.67.

**[Fe<sub>2</sub>( $\mu$ -O<sub>2</sub>CAr<sup>FPh</sup>)<sub>4</sub>(4-<sup>t</sup>BuC<sub>5</sub>H<sub>4</sub>N)<sub>2</sub>] (12).** This compound was prepared in a manner similar to that described for **10**, except that 4-*tert*-butylpyridine was used instead of pyridine. Greenish yellow blocks of **12** (62%) were obtained by vapor diffusion of pentanes into the reaction mixture and analyzed by X-ray crystallography. FT-IR (KBr,  $\text{cm}^{-1}$ ): 3057, 2966, 2905, 2870, 1614, 1580, 1554, 1510, 1452, 1403, 1382, 1222, 1159, 1095, 1074, 844, 831, 818, 793, 772, 727, 706, 555, 530, 468. UV-vis ( $\text{CH}_2\text{Cl}_2$ ,  $\lambda_{\text{max}}$ , nm ( $\epsilon$ ,  $\text{M}^{-1}\text{cm}^{-1}$ ): 365 (1200). Anal. Calcd for  $\text{C}_{94}\text{H}_{70}\text{N}_2\text{O}_8\text{F}_8\text{Fe}_2$ : C, 69.72; H, 4.36; N, 1.73. Found: C, 69.97; H, 4.45; N, 1.64.

**X-ray Crystallographic Studies.** Intensity data were collected on a Bruker (formerly Siemens) CCD diffractometer with graphite-monochromated Mo  $\text{K}\alpha$  radiation ( $\lambda = 0.71073 \text{ \AA}$ ), controlled by a Pentium-based PC running the SMART software package.<sup>40</sup> Single crystals were mounted at room temperature on the tips of quartz fibers, coated with Paratone-N oil, and cooled to 188 K under a stream of cold nitrogen maintained by a Bruker LT-2A nitrogen cryostat. Data collection and reduction protocols are described elsewhere.<sup>41</sup> The structures were solved by direct methods and refined on  $F^2$  by using the SHELXTL software package.<sup>42</sup> Empirical absorption corrections were applied with SADABS,<sup>43</sup> part of the SHELXTL program package, and the structures were checked for higher symmetry by the PLATON program.<sup>44</sup> All non-hydrogen atoms were refined anisotropically unless otherwise noted. Hydrogen atoms were assigned idealized positions and given thermal parameters equivalent to either 1.5 (methyl hydrogen atoms) or 1.2 (all other hydrogen atoms) times the thermal parameter of the carbon atom to which they were attached. The hydrogen atoms associated with the disordered solvent molecules were not included in the

(40) SMART v5.05: Software for the CCD Detector System; Bruker AXS: Madison, WI, 1998.

(41) Feig, A. L.; Bautista, M. T.; Lippard, S. J. *Inorg. Chem.* **1996**, *35*, 6892–6898.

(42) Sheldrick, G. M. SHELXTL97–2: Program for the Refinement of Crystal Structures; University of Göttingen: Göttingen, Germany, 1997.

(43) Sheldrick, G. M. SADABS: Area-Detector Absorption Correction; University of Göttingen: Göttingen, Germany, 1996.

(44) Spek, A. L. PLATON, A Multipurpose Crystallographic Tool; Utrecht University: Utrecht, The Netherlands, 1998.

refinement. The THF ligands in **1** were disordered over two positions. The occupancy of four carbons was equally distributed and refined isotropically. A disordered CH<sub>2</sub>Cl<sub>2</sub> molecule in the structure of **2** was distributed over two positions and refined. The disordered MeCN and CH<sub>2</sub>Cl<sub>2</sub> solvent molecules in the structure of **3** were equally distributed over two positions and refined isotropically. The lattice solvent molecules in the structure of **5** were modeled as partially occupied CH<sub>2</sub>Cl<sub>2</sub> (0.75 occupancy) and pentane (0.25 occupancy). The *tert*-butyl group on each 4-*tert*-butylpyridine in the structure of **7** is distributed over two positions and refined isotropically. In the structure of **8** each coordinated THF molecule was disordered over two positions. In each case, two of the carbon atoms and the oxygen atom were refined at full occupancy, and the occupancies of the remaining two carbon atoms were equally distributed over two positions and refined isotropically. The THF ligands in **9** were disordered over two positions. In one molecule, three carbon atoms were distributed at 0.7 and 0.3 occupancies and refined. In the other, the occupancy of four carbon atoms was distributed at 0.7 and 0.3 occupancies and refined isotropically. One of the chlorine atoms in the disordered CH<sub>2</sub>Cl<sub>2</sub> molecule was equally distributed over two positions. Three carbon atoms of a disordered pentane molecule were distributed at 0.6 and 0.4 occupancies and refined. A disordered CH<sub>2</sub>Cl<sub>2</sub> molecule in the structure of **10** was equally distributed over two positions and refined isotropically. The other CH<sub>2</sub>Cl<sub>2</sub> molecule was refined with 0.8 and 0.2 occupancies. Each of the three CH<sub>2</sub>Cl<sub>2</sub> solvent molecules in the structure of **11** was distributed over two positions with equal occupancies. One carbon atom of a lattice solvent Et<sub>2</sub>O in **12** was equally distributed over two positions and refined isotropically. Crystallographic information is provided in Table S1, and Figures S1–S10 display ORTEP diagrams of the molecular structures (Supporting Information).

**<sup>57</sup>Fe Mössbauer Spectroscopy.** Mössbauer spectra of **2**, **4**, **5**, and **7** were obtained on an MS1 spectrometer (WEB Research Co.) with a <sup>57</sup>Co source in a Rh matrix maintained at room temperature in the MIT Department of Chemistry Instrumentation Facility. Solid samples were prepared by suspending ~0.04 mmol of the powdered material in Apeizon N grease and packing the mixture into a nylon sample holder. All data were collected at 4.2 K, and the isomer shift ( $\delta$ ) values are reported with respect to natural iron foil that was used for velocity calibration at room temperature. The spectra were fit to Lorentzian lines by using the WMOSS plot and fit program.<sup>45</sup>

**Magnetic Susceptibility.** Magnetic susceptibility data for polycrystalline powders of **4**, **5**, and **7** were measured between 5 and 300 K with applied magnetic fields of 0.5 T using a Quantum Design MPMS SQUID susceptometer. Samples were loaded in gel capsules under nitrogen and suspended in plastic straws. Data were corrected for the magnetism of the sample holder, which was independently determined at the same temperature range and field. Underlying diamagnetism of the sample was estimated from Pascal's constants.<sup>46</sup> The molar magnetic susceptibility data were fit to the expression derived from the spin-only isotropic HDvV exchange Hamiltonian  $\mathcal{H} = -2JS_1S_2$ , where  $S_1 = S_2 = 2$ . This expression is given in eq 1, where  $x = J/kT$ . No corrections were made for TIP or paramagnetic impurities.

$$\chi_M = \frac{Ng^2\mu_B^2}{kT} \frac{2e^{2x} + 10e^{6x} + 28e^{12x} + 60e^{20x}}{1 + 3e^{2x} + 5e^{6x} + 7e^{12x} + 9e^{20x}} \quad (1)$$

## Results

**Ligand Synthesis and Initial Metalation Attempts.** A tandem benzyne generation–nucleophilic capture–electro-

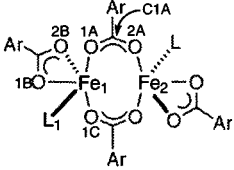
philic quench protocol, involving a modification<sup>39b</sup> of the Hart reaction,<sup>39a</sup> afforded gram quantities of Ar'CO<sub>2</sub>H (Ar' = Ar<sup>Tol</sup> or Ar<sup>4-FPh</sup>) as crystalline solids. The corresponding metal salts, MO<sub>2</sub>CAr' (M = Tl or Na), were readily obtained by treating the free acid with either TIOEt or NaOH. They were used in anion metathesis reactions with FeBr<sub>2</sub> or Fe(OTf)<sub>2</sub>·2MeCN in anhydrous THF. When reactions between FeBr<sub>2</sub> and 2 equiv of TlO<sub>2</sub>CAr<sup>Tol</sup> were conducted for less than ~3 h in THF, yellow blocks of [Fe<sub>2</sub>( $\mu$ -O<sub>2</sub>CAr<sup>Tol</sup>)<sub>2</sub>(THF)<sub>2</sub>Br<sub>2</sub>] (**1**) were obtained following recrystallization from CH<sub>2</sub>Cl<sub>2</sub>/pentanes. The crystal structure of **1** is shown in Figure S1; selected bond lengths and angles are listed in Table 1. The two iron atoms in **1** are connected by two  $\mu$ -1,3-bridging carboxylate ligands that span an Fe···Fe distance of 3.5684(13) Å. Terminal bromide and THF ligands complete the pseudotetrahedral coordination of iron. Since **1** did not contain the desired {Fe<sub>2</sub>(O<sub>2</sub>CAr<sup>Tol</sup>)<sub>4</sub>} unit, it was not further characterized.

**Synthesis and Structural Characterization of Doubly Bridged Diiron(II) Complexes [Fe<sub>2</sub>( $\mu$ -O<sub>2</sub>CAr<sup>Tol</sup>)<sub>2</sub>(O<sub>2</sub>CAr<sup>Tol</sup>)<sub>2</sub>L<sub>2</sub>], L = THF (**2**), MeCN (**3**), Pyridine (**4**), and 1-MeIm (**5**).** Compound **2** was prepared in good yield (~77%) from a reaction between FeBr<sub>2</sub> and 2 equiv of TlO<sub>2</sub>CAr<sup>Tol</sup> in anhydrous THF. An extended reaction period (>10 h) was required for complete metathesis of bromide with the carboxylate ligands (vide supra). The two five-coordinate iron atoms in **2** are related by a crystallographic inversion center (Scheme 1). The relatively long Fe···Fe separation of 4.2822(7) Å is spanned by two bridging carboxylate ligands (Table 1). The remaining coordination sites are occupied by THF and bidentate terminal carboxylate ligands, which complete the distorted trigonal bipyramidal coordination geometry. The same air-sensitive compound can be prepared in comparable yield (~67%) from Fe(OTf)<sub>2</sub>·2MeCN and 2 equiv of NaO<sub>2</sub>CAr<sup>Tol</sup> in THF.

The weakly bound THF molecules in **2** can be readily displaced by N-donor ligands (L), allowing access to derivatives sharing the common molecular formula [Fe<sub>2</sub>( $\mu$ -O<sub>2</sub>CAr<sup>Tol</sup>)<sub>2</sub>(O<sub>2</sub>CAr<sup>Tol</sup>)<sub>2</sub>L<sub>2</sub>] (Scheme 1). Simply by recrystallizing **2** in a mixture of MeCN/CH<sub>2</sub>Cl<sub>2</sub>/pentanes, we obtained **3** (Figure S2) in good yield (~79%). Two essentially identical dinuclear complexes were identified in the crystallographic asymmetric unit, for which comparable Fe···Fe distances of 3.9602(13) and 3.9754(12) Å were observed. Upon treating a CH<sub>2</sub>Cl<sub>2</sub> solution of **2** with 2 equiv of pyridine, the reaction mixture turned intense yellow, and pale ivory microcrystals of **4** immediately deposited. As shown in Figures 2 and 3, a crystallographic inversion center in **4** requires the two iron and four oxygen atoms of the  $\mu$ -1,3 carboxylates to lie in the same plane. Two pyridine and two terminal carboxylate ligands are disposed anti to each other across this {Fe<sub>2</sub>O<sub>4</sub>} plane, a situation similar to that in **2** and **3**. When **2** was allowed to react with 2 equiv of 1-methylimidazole (1-MeIm), colorless crystals of **5** were obtained following recrystallization from CH<sub>2</sub>Cl<sub>2</sub>/pentanes.

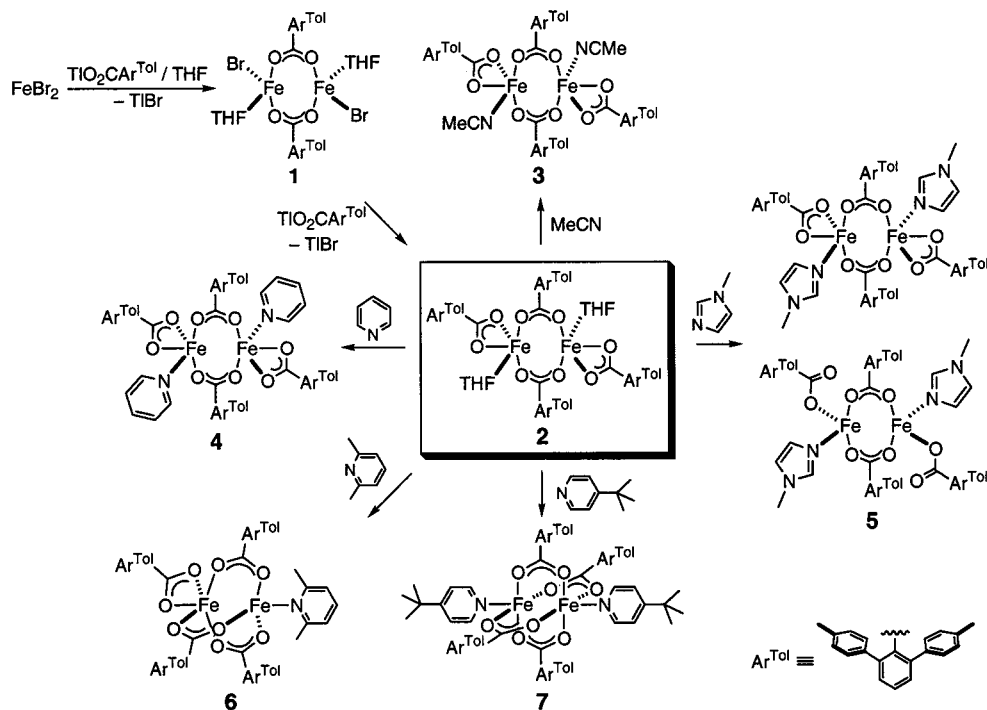
(45) Kent, T. A. *WMOSS v2.5: Mössbauer Spectral Analysis Software*; WEB Research Co.: Minneapolis, MN, 1998.

(46) Carlin, R. L. *Magnetochemistry*; Springer-Verlag: New York, 1986.

**Table 1.** Selected Bond Lengths (Å) and Angles (deg) for **1–5** and **8<sup>a</sup>**


	<b>1</b>	<b>2</b>	<b>3</b>	<b>4</b>	<b>5</b>	<b>8</b>
Fe1...Fe2	3.5684(13)	4.2822(7)	3.9754(12) <sup>b</sup> 3.9602(13) <sup>c</sup>	4.2189(13)	4.2029(10) <sup>d</sup> 4.1967(11) <sup>e</sup>	4.1869(9) <sup>d</sup> 4.1452(8) <sup>e</sup>
Fe1–O1A	1.967(3)	1.9428(19)	1.920(3) <sup>b</sup> 1.910(3) <sup>c</sup>	1.957(3)	1.950(3) <sup>d</sup> 1.980(3) <sup>e</sup>	1.949(2) <sup>d</sup> 1.968(2) <sup>e</sup>
Fe1–O1C <sup>f</sup>	1.995(3)	2.0061(18)	1.994(3) <sup>b</sup> 2.000(3) <sup>c</sup>	2.006(3)	2.015(3) <sup>d</sup> 2.017(3) <sup>e</sup>	1.993(2) <sup>d</sup> 1.995(2) <sup>e</sup>
Fe1–O1B		2.0363(19)	2.048(2) <sup>b</sup> 2.049(3) <sup>c</sup>	2.047(3)	2.025(3) <sup>d</sup> 2.090(3) <sup>e</sup>	1.980(2) <sup>d</sup> 2.029(2) <sup>e</sup>
Fe1–O2B		2.3455(19)	2.327(2) <sup>b</sup> 2.318(2) <sup>c</sup>	2.358(3)	2.463(3) <sup>d,g</sup> 2.315(3) <sup>e</sup>	2.661(3) <sup>d,g</sup> 2.342(2) <sup>e</sup>
Fe1–L1	2.040(3) <sup>h</sup>	2.0941(19)	2.123(3) <sup>b</sup> 2.130(3) <sup>c</sup>	2.132(4)	2.092(3) <sup>d</sup> 2.085(3) <sup>e</sup>	2.088(2) <sup>d</sup> 2.082(2) <sup>e</sup>
Fe1–O1A–C1A	136.8(3)	156.64(19)	155.4(3) <sup>b</sup> 159.1(3) <sup>c</sup>	152.8(3)	153.9(3) <sup>d</sup> 140.0(3) <sup>e</sup>	147.4(2) <sup>d</sup> 151.2(2) <sup>e</sup>
Fe2–O2A–C1A	129.2(3)	135.98(18)	129.2(3) <sup>b</sup> 127.3(3) <sup>c</sup>	135.6(3)	137.0(2) <sup>d</sup> 147.9(3) <sup>e</sup>	140.9(2) <sup>d</sup> 132.0(2) <sup>e</sup>

<sup>a</sup> Numbers in parentheses are estimated standard deviations of the last significant figures. <sup>b</sup> Molecule 1 in the asymmetric unit. <sup>c</sup> Molecule 2 in the asymmetric unit. <sup>d</sup> 4,4-Coordinate isomer. <sup>e</sup> 5,5-Coordinate isomer. <sup>f</sup> Fe1–O1C and Fe2–O2A are identical. <sup>g</sup> Fe...O<sub>non-coordinating</sub>. <sup>h</sup> Fe–O<sub>THF</sub>.

**Scheme 1**

X-ray structure analysis revealed two chemically equivalent but crystallographically inequivalent molecules of **5** in the unit cell. In one molecule, the terminal carboxylates are bidentate chelating, as in **2**, **3**, and **4**, whereas these ligands have undergone carboxylate shifts to afford monodentate terminal coordination and four-coordinate iron centers in the other molecule (Figure 2). The Fe...Fe separation is not significantly affected by this structural variation. Comparable intermetallic distances of 4.2029(10) and 4.1967(11) Å were obtained for the 4,4-coordinate and 5,5-coordinate complex, respectively. Selected bond lengths and angles in **2–5** are

listed in Table 1. Strict exclusion of TlO<sub>2</sub>CAr<sup>Tol</sup> impurity from the reaction mixture is essential for the preparation of pure **4** and **5**. When similar synthetic procedures were followed by using a crude batch of **2**, heterodimetallic complexes [FeTl(μ-O<sub>2</sub>CAr<sup>Tol</sup>)<sub>3</sub>L] (L = C<sub>5</sub>H<sub>5</sub>N or 1-MeIm) were isolated. The structures of these compounds were determined by X-ray crystallography (Figures S3 and S4).<sup>47,48</sup>

(47) Crystal data for [FeTl(μ-O<sub>2</sub>CAr<sup>Tol</sup>)<sub>3</sub>(C<sub>5</sub>H<sub>5</sub>N)]: space group *P* $\bar{1}$  with *a* = 11.097(2) Å, *b* = 23.499(4) Å, *c* = 25.524(9) Å,  $\alpha$  = 68.759(14)°,  $\beta$  = 78.926(14)°,  $\gamma$  = 85.259(12)°, *V* = 6088(3) Å<sup>3</sup>, *Z* = 4, *R* = 0.0520, *wR*<sup>2</sup> = 0.1452.

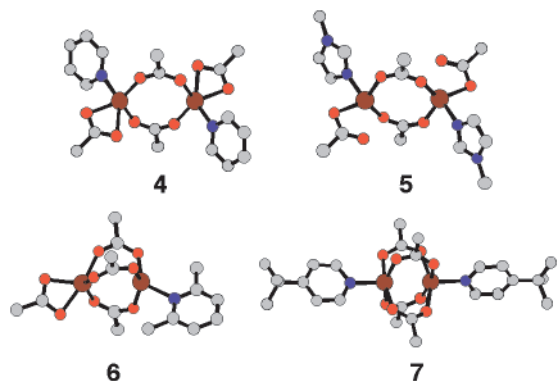


**Figure 2.** Ball and stick representation of the solid state structures of  $[\text{Fe}_2(\mu\text{-O}_2\text{CAR}^{\text{Tot}})_2(\text{O}_2\text{CAR}^{\text{Tot}})_2(\text{C}_5\text{H}_5\text{N})_2]$  (**4**),  $[\text{Fe}_2(\mu\text{-O}_2\text{CAR}^{\text{Tot}})_2(\text{O}_2\text{CAR}^{\text{Tot}})_2(1\text{-MeIm})_2]$  (**5**),  $[\text{Fe}_2(\mu\text{-O}_2\text{CAR}^{\text{Tot}})_3(\text{O}_2\text{CAR}^{\text{Tot}})(2,6\text{-lutidine})]$  (**6**), and  $[\text{Fe}_2(\mu\text{-O}_2\text{CAR}^{\text{Tot}})_4(4\text{-}^t\text{BuC}_5\text{H}_4\text{N})_2]$  (**7**) generated using the crystallographic coordinates. For clarity, all atoms of the  $\text{Ar}^{\text{Tot}}\text{CO}_2^-$  ligand, except for the carboxylate groups and the  $\alpha$ -carbon atoms, were omitted.

**Synthesis and Structural Characterization of Triply and Quadruply Bridged Diiron(II) Complexes  $[\text{Fe}_2(\mu\text{-O}_2\text{CAR}^{\text{Tot}})_3(\text{O}_2\text{CAR}^{\text{Tot}})(2,6\text{-lutidine})]$  (**6**) and  $[\text{Fe}_2(\mu\text{-O}_2\text{CAR}^{\text{Tot}})_4(4\text{-}^t\text{BuC}_5\text{H}_4\text{N})_2]$  (**7**).** A triply bridged diiron(II) complex **6** was obtained by treating a  $\text{CH}_2\text{Cl}_2$  solution of **2** with 2,6-lutidine. Even when an excess ( $> 10$  equiv) amount of 2,6-lutidine was used, only 1 equiv of the N-donor ligand was incorporated upon displacement of two THF molecules from **2**. The crystal structure of **6** is shown in Figures 2 and S5; selected bond distances and angles are available in Table 2. Unlike the di( $\mu$ -carboxylato)diiron(II) complexes **2–5**, in **6** the two iron atoms are not symmetry-related, but are bridged by three  $\mu$ -1,3 carboxylate ligands. The  $\text{Fe}\cdots\text{Fe}$  distance of 3.2342(4) Å is significantly shorter than those (3.9602(13)–4.2822(7) Å) in the windmill complexes **2–5**.

Substitution of THF ligands in **2** with 2 equiv of 4-*tert*-butylpyridine afforded the paddlewheel compound **7**. Air-sensitive yellow blocks of **7** were obtained following recrystallization from  $\text{CH}_2\text{Cl}_2/\text{Et}_2\text{O}$ . The same compound can be directly prepared by a reaction between  $\text{Fe}(\text{OTf})_2\cdot 2\text{MeCN}$ ,  $\text{NaO}_2\text{CAR}^{\text{Tot}}$ , and 4-*tert*-butylpyridine in a 1:2:1 ratio. The crystal structure of **7** is depicted in Figure 2; selected bond distances and angles are listed in Table 2. The  $\text{Fe}\cdots\text{Fe}$  distance is 2.8229(9) Å, and there are four  $\mu$ -1,3 carboxylate ligands disposed around a pseudo- $C_4$  axis along the Fe–Fe vector. The crystallographically inequivalent iron(II) centers have similar square pyramidal coordination geometries with comparable average Fe–O distances of 2.09(6) Å for Fe(1) and 2.09(7) Å for Fe(2).

**Doubly and Quadruply Bridged Diiron(II) Complexes Having Identical Ligand Combinations: Synthesis and Structural Characterization of  $[\text{Fe}_2(\mu\text{-O}_2\text{CAR}^{4\text{-FPh}})_2(\text{O}_2\text{CAR}^{4\text{-FPh}})_2(\text{THF})_2]$  (**8**) and  $[\text{Fe}_2(\mu\text{-O}_2\text{CAR}^{4\text{-FPh}})_4(\text{THF})_2]$  (**9**).** Reaction of  $\text{Fe}(\text{OTf})_2\cdot 2\text{MeCN}$  with 2 equiv of  $\text{NaO}_2\text{CAR}^{4\text{-FPh}}$  in anhydrous THF afforded colorless blocks of **8** in modest yield ( $\sim 50\%$ ). The crystal structure of **8** is

shown in Figure S6; selected bond lengths and angles are listed in Table 1. The lateral width occupied by the *m*-terphenyl unit is diminished when the 2,6-substituents are changed from *p*-tolyl to 4-fluorophenyl groups. The corresponding van der Waals radii of  $\text{CH}_3$  and F are 2.0 and 1.47 Å, respectively.<sup>49,50</sup> The solid state geometry of **8**, however, is similar to that of the analogous THF complex **2** prepared from  $\text{Ar}^{\text{Tot}}\text{CO}_2^-$ , suggesting that the steric properties of  $\text{Ar}^{4\text{-FPh}}\text{CO}_2^-$  are comparable to those of  $\text{Ar}^{\text{Tot}}\text{CO}_2^-$ . Unlike **2**, two chemically equivalent dinuclear units of **8** were identified in the unit cell. In one molecule, the terminal carboxylate ligands are bidentate, affording five-coordinate iron centers. In the other molecule, monodentate coordination of terminal carboxylate renders the iron centers four-coordinate. The metal $\cdots$ metal separation is not significantly affected by this structural variation, as indicated by the comparable intermetallic distances of 4.1869(9) and 4.1452(8) Å observed for the 4,4-coordinate and 5,5-coordinate complexes, respectively.

A paddlewheel diiron(II) compound **9** was obtained as a product of an unsuccessful attempt to oxidize **8** with 2 equiv of  $[\text{Cp}_2\text{Fe}](\text{PF}_6)$  in  $\text{CH}_2\text{Cl}_2$ . Pale green blocks were obtained by recrystallization from  $\text{CH}_2\text{Cl}_2/\text{pentanes}$  and analyzed by X-ray crystallography. The crystal structure of **9** is shown in Figure S7; selected bond lengths and angles are listed in Table 2. As in **7**, there are four bridging carboxylate ligands related by a pseudo- $C_4$  axis along the Fe–Fe vector. The metal $\cdots$ metal distance of 2.7277(7) Å is significantly shorter than those of the doubly bridged dimetallic cores in the precursor complex **8**. Although further characterization of this compound was hampered by contamination with unidentified dark-colored materials, the structure of **9** clearly indicates that both windmill and paddlewheel isomers of a diiron(II) complex can be accessed from an identical ligand set, and their interconversion is likely to occur in solution (vide infra).

**Synthesis and Structural Characterization of Quadruply Bridged Diiron(II) Complexes  $[\text{Fe}_2(\mu\text{-O}_2\text{CAR}^{4\text{-FPh}})_4\text{L}_2]$ ,  $\text{L} = \text{C}_5\text{H}_5\text{N}$  (**10**), 1-MeIm (**11**), and 4- $^t\text{BuC}_5\text{H}_4\text{N}$  (**12**).** Neutral paddlewheel diiron(II) compounds **10–12** were conveniently prepared by ligand substitution of **8** with 2 equiv of the appropriate N-donor ligand (Scheme 2). Recrystallization from  $\text{CH}_2\text{Cl}_2/\text{pentanes}$  afforded X-ray quality crystalline materials in modest yields (44–67%). The crystal structures of **10–12** are shown in Figures S8–S10; selected bond distances and angles are listed in Table 2. The metal centers in **10–12** all have square pyramidal geometry similar to that of the  $\text{Ar}^{\text{Tot}}\text{CO}_2^-$ -supported analogue **7**. All metric parameters are normal, and the  $\text{Fe}\cdots\text{Fe}$  distances range from 2.8247(5) to 2.8475(7) Å.

**Mössbauer Spectroscopy.** Zero-field Mössbauer spectra of solid samples of **2**, **4**, **5**, and **7** were collected at 4.2 K. Figures 4 and S11 (Supporting Information) display the spectra; the corresponding parameters derived from fits of the spectra are provided in Table 3 along with those of related

(48) Crystal data for  $[\text{FeTi}(\mu\text{-O}_2\text{CAR}^{\text{Tot}})_3(1\text{-MeIm})]$ : space group  $P\bar{1}$  with  $a = 13.9499(3)$  Å,  $b = 14.8627(3)$  Å,  $c = 15.2549(2)$  Å,  $\alpha = 88.374(1)^\circ$ ,  $\beta = 87.776(1)^\circ$ ,  $\gamma = 83.896(1)^\circ$ ,  $V = 3141.6(1)$  Å<sup>3</sup>,  $Z = 2$ ,  $R = 0.0457$ ,  $wR^2 = 0.1319$ .

(49) Bondi, A. *J. Phys. Chem.* **1964**, *68*, 441–451.

(50) Pauling, L. *The Nature of the Chemical Bond*, 3rd ed.; Cornell University Press: Ithaca, NY, 1960.

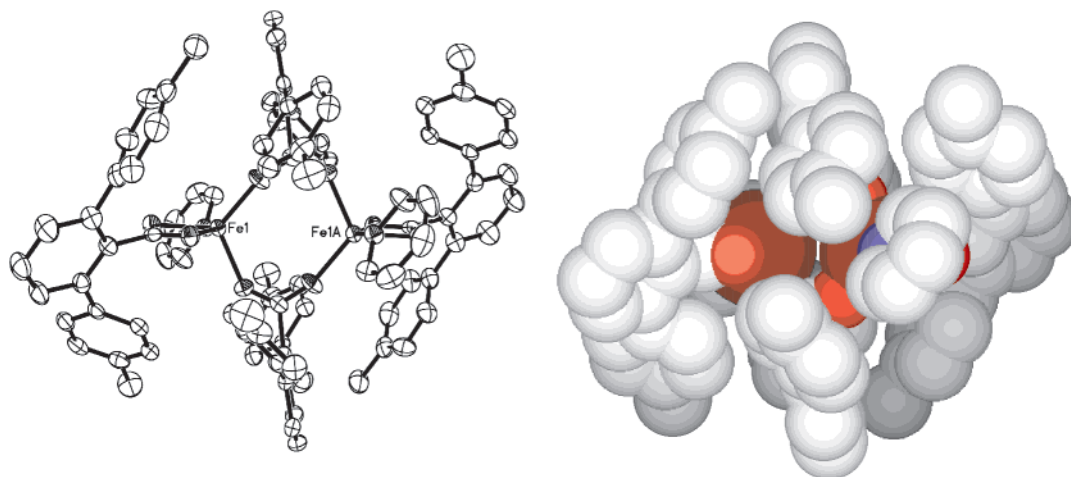
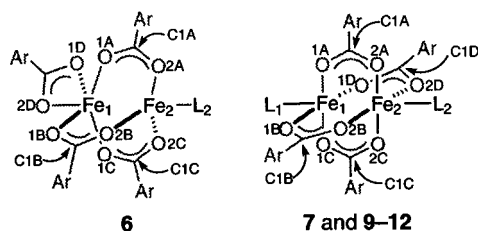


**Figure 3.** Solid state structure of  $[\text{Fe}_2(\mu\text{-O}_2\text{CAr}^{\text{Tol}})_2(\text{O}_2\text{CAr}^{\text{Tol}})_2(\text{C}_5\text{H}_5\text{N})_2]$  (**4**): left, ORTEP diagram with thermal ellipsoids at 50% probability; right, space-filling representation, where N is blue, O is bright red, and Fe is dark red.

**Table 2.** Selected Bond Lengths (Å) and Angles (deg) for **6**, **7**, and **9–12**<sup>a</sup>



	<b>6</b>	<b>7</b>	<b>9</b>	<b>10</b>	<b>11</b>	<b>12</b>
Fe1...Fe2	3.2342(4)	2.8229(9)	2.7277(7)	2.8249(9)	2.8475(7)	2.8247(5)
Fe1–O1A	2.0698(14)	2.136(3)	2.060(2)	2.196(3)	2.162(3)	2.1165(19)
Fe1–O1B	2.0645(15)	2.031(3)	2.061(2)	2.161(3)	2.208(3)	2.0526(19)
Fe1–O1C	2.0443(15)	2.028(3)	2.072(2)	2.031(3)	2.039(3)	2.0383(19)
Fe1–O1D	2.0776(15)	2.145(3)	2.079(2)	2.033(3)	2.036(2)	2.1152(19)
Fe1–O2D	2.2137(14)					
Fe1–L1		2.105(4)	2.041(3)	2.094(4)	2.068(3)	2.098(2)
Fe2–O2A	1.9968(14)	2.026(3)	2.155(2)	2.018(3)	2.024(3)	2.0460(19)
Fe2–O2B	1.9836(15)	2.160(3)	2.068(2)	2.012(3)	2.024(3)	2.1278(19)
Fe2–O2C	1.9968(14)	2.156(3)	2.075(2)	2.135(3)	2.156(3)	2.1174(19)
Fe2–O2D		2.034(3)	2.101(2)	2.129(3)	2.151(3)	2.0507(18)
Fe2–L2	2.1102(17)	2.098(4)	2.038(3)	2.081(4)	2.066(3)	2.086(2)
Fe1–O1A–C1A	127.58(13)	119.1(3)	121.1(2)	120.0(3)	112.9(2)	118.20(18)
Fe1–O1B–C1B	132.63(14)	130.4(3)	125.5(2)	113.2(3)	127.5(2)	130.23(17)
Fe1–O1C–C1C	142.78(15)	132.2(3)	121.6(2)	131.1(3)	128.4(2)	130.15(18)
Fe1–O1D–C1D		117.4(3)	127.1(2)	126.2(3)	131.5(2)	118.48(17)
Fe2–O2A–C1A	130.16(13)	130.9(3)	122.7(2)	127.3(3)	135.9(2)	129.45(18)
Fe2–O2B–C1B	126.71(13)	117.4(3)	120.7(2)	136.3(3)	127.5(2)	117.84(17)
Fe2–O2C–C1C	115.68(14)	115.2(3)	123.1(2)	116.7(3)	119.1(2)	117.81(18)
Fe2–O2D–C1D		130.9(3)	118.0(2)	121.2(3)	116.3(2)	128.72(17)

<sup>a</sup> Numbers in parentheses are estimated standard deviations of the last significant figures.

diiron(II) centers in non-heme enzymes.<sup>9,11,51–55</sup> Compounds **2** and **4** exhibit single sharp ( $\Gamma = 0.25\text{--}0.28\text{ mm s}^{-1}$ ) quadrupole doublets, consistent with two iron centers related by a crystallographic inversion center. Although there are two crystallographically unique iron sites in **7**, their nearly

identical coordination environments produce unresolved Mössbauer spectra with a sharp ( $\Gamma = 0.24\text{--}0.26\text{ mm s}^{-1}$ ) quadrupole doublet. Significant broadening of the peaks ( $\Gamma = 0.34\text{--}0.40\text{ mm s}^{-1}$ ) occurs for **5**, however, which exists in two crystallographically inequivalent dinuclear units in the solid state (vide supra). No attempt was made to deconvolute the unresolved quadrupole doublet into contributions from the 4,4-coordinate and 5,5-coordinate components. The isomer shifts and quadrupole splittings of **2**, **4**, **5**, and **7** are typical of high-spin iron(II) sites in a N/O coordination

(51) Pulver, S.; Froland, W. A.; Fox, B. G.; Lipscomb, J. D.; Solomon, E. I. *J. Am. Chem. Soc.* **1993**, *115*, 12409–12422.

(52) Fox, B. G.; Hendrich, M. P.; Surerus, K. K.; Andersson, K. K.; Froland, W. A.; Lipscomb, J. D.; Münck, E. *J. Am. Chem. Soc.* **1993**, *115*, 3688–3701.

(53) Lynch, J. B.; Juarez-Garcia, C.; Münck, E.; Que, L., Jr. *J. Biol. Chem.* **1989**, *264*, 8091–8096.

(54) Pulver, S. C.; Tong, W. H.; Bollinger, M. J., Jr.; Stubbe, J.; Solomon, E. I. *J. Am. Chem. Soc.* **1995**, *117*, 12664–12678.

(55) Fox, B. G.; Shanklin, J.; Somerville, C.; Münck, E. *Proc. Natl. Acad. Sci. U.S.A.* **1993**, *90*, 2486–2490.



Scheme 2

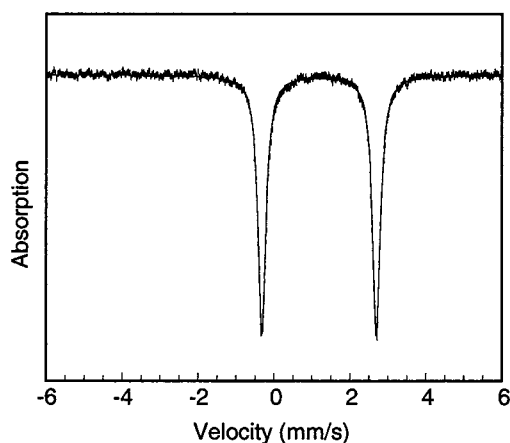
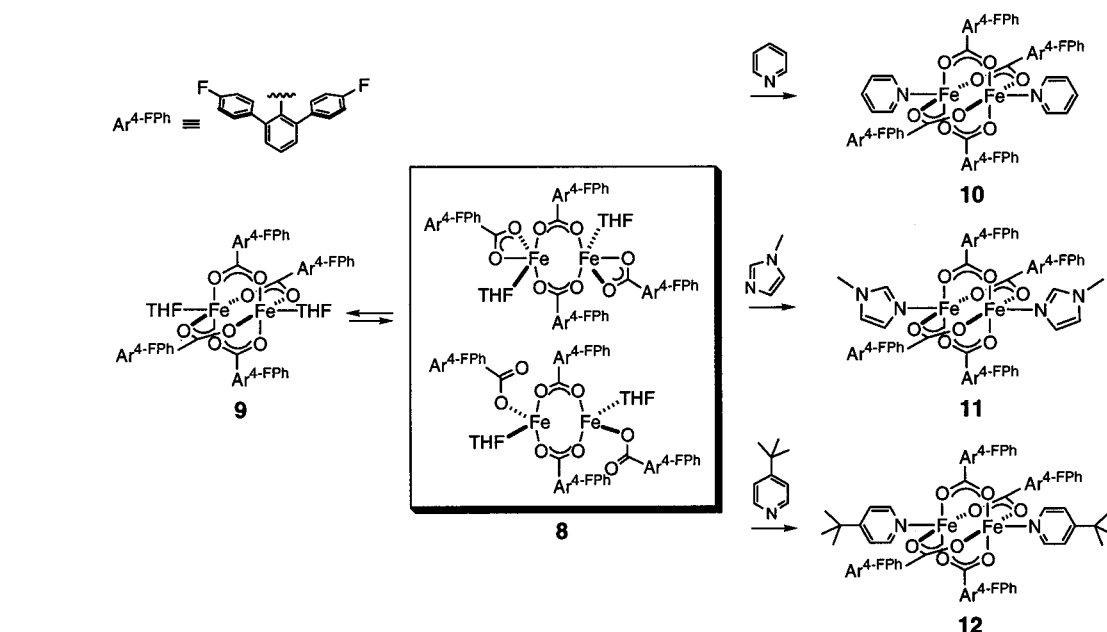


**Figure 4.** Zero-field Mössbauer spectrum (experimental data (—), calculated fit (---)) recorded at 4.2 K for  $[\text{Fe}_2(\mu\text{-O}_2\text{CAr}^{\text{Tol}})_2(\text{O}_2\text{CAr}^{\text{Tol}})_2\text{-}(\text{C}_5\text{H}_5\text{N})_2]$  (**4**) in the solid state. See Table 3 for derived Mössbauer parameters.

environment<sup>18,56,57</sup> and comparable to those obtained for related biological clusters (Table 3).<sup>1b,1f</sup> The similar Mössbauer parameters obtained for **2**, **4**, and **5** suggest that the electronic environment around the metal center is not significantly perturbed upon ligand substitution within the  $[\text{Fe}_2(\mu\text{-O}_2\text{CAr}^{\text{Tol}})_2(\text{O}_2\text{CAr}^{\text{Tol}})_2\text{L}_2]$  module.

**Magnetic Susceptibility Studies.** The two iron(II) centers in the di( $\mu$ -carboxylato)diiron(II) compounds **4** and **5** display similarly weak antiferromagnetic (AF) coupling. Plots of the effective magnetic moment ( $\mu_{\text{eff}}$ ) and molar susceptibility ( $\chi_{\text{M}}$ ) versus temperature for **4** and **5** are shown in Figures 5 and S12 (Supporting Information). The measured values of  $\mu_{\text{eff}} = 7.60$  (for **4**) and  $7.45 \mu_{\text{B}}$  (for **5**) at 300 K are close to

the theoretical value of  $7.62 \mu_{\text{B}}$  calculated for the effective moment of two uncoupled  $S = 2$  centers with  $g = 2.2$ .<sup>58</sup> Upon lowering the temperature,  $\mu_{\text{eff}}$  gradually decreases to ca.  $7.0 \mu_{\text{B}}$  at 50 K, below which it rapidly drops to  $4.14$  and  $3.72 \mu_{\text{B}}$  at 5 K for **4** and **5**, respectively. These relatively high  $\mu_{\text{B}}$  values indicate that excited magnetic states are still populated at the lowest temperature.

The magnetic susceptibility data were fit by using an expression derived from the spin-only isotropic HDvV exchange Hamiltonian  $\mathcal{H} = -2JS_1 \cdot S_2$ , where  $S_1 = S_2 = 2$ . The best fit was obtained for  $J = -0.90(3) \text{ cm}^{-1}$  and  $g = 2.16(1)$  for **4** (Figure 5). Similar treatment afforded  $J = -1.04(2) \text{ cm}^{-1}$  and  $g = 2.14(1)$  for **5** (Figure S12). This simplified analysis, however, does not take into account spin-orbit coupling and zero-field splitting (ZFS). Although the orbital contribution is significantly quenched with a deviation from ideal octahedral geometry,<sup>59</sup> ZFS of iron(II) complexes can be on the same order of magnitude as the exchange coupling.<sup>60</sup> This effect would result in a complicated energy level distribution. Given these features, it should be noted that the calculated fit may not be a unique solution for the observed magnetic behavior. Nevertheless, the weak AF coupling interaction exhibited by **4** and **5** is consistent with the absence of a more efficient exchange pathway between two iron(II) centers separated by  $> 4 \text{ \AA}$ . Parameters derived from fits of the curves are provided in Table 3 along with those of related diiron(II) centers in the biological systems.

The magnetic behavior of the paddlewheel diiron(II) compound **7**, however, is significantly different from that of **4** and **5**. The  $\mu_{\text{eff}}$  vs  $T$  as well as  $\chi_{\text{M}}$  vs  $T$  curves for **7** are

(56) Gütllich, P.; Enslin, J. In *Inorganic Electronic Structure and Spectroscopy*; Solomon, E. I., Lever, A. B. P., Eds.; John Wiley & Sons: New York, 1999; Vol. I, pp 161–211.

(57) Münck, E. In *Physical Methods in Bioinorganic Chemistry: Spectroscopy and Magnetism*; Que, L., Jr., Ed.; University Science Books: Sausalito, CA, 2000; pp 287–319.

(58) Girerd, J.-J.; Journaux, Y. In *Physical Methods in Bioinorganic Chemistry: Spectroscopy and Magnetism*; Que, L., Jr., Ed.; University Science Books: Sausalito, CA, 2000; pp 321–374.

(59) Borrás-Almenar, J. J.; Clemente-Juan, J. M.; Coronado, E.; Pali, A. V.; Tsukerblat, B. S. *J. Phys. Chem. A* **1998**, *102*, 200–213.

(60) Varet, F. *J. Phys. Chem. Solids* **1976**, *37*, 257–263.

**Table 3.** Mössbauer and Magnetic Parameters for  $[\text{Fe}_2(\mu\text{-O}_2\text{CAr}^{\text{Tot}})_2(\text{O}_2\text{CAr}^{\text{Tot}})_2(\text{THF})_2]$  (**2**),  $[\text{Fe}_2(\mu\text{-O}_2\text{CAr}^{\text{Tot}})_2(\text{O}_2\text{CAr}^{\text{Tot}})_2(\text{C}_5\text{H}_5\text{N})_2]$  (**4**),  $[\text{Fe}_2(\mu\text{-O}_2\text{CAr}^{\text{Tot}})_2(\text{O}_2\text{CAr}^{\text{Tot}})_2(1\text{-MeIm})_2]$  (**5**),  $[\text{Fe}_2(\mu\text{-O}_2\text{CAr}^{\text{Tot}})_4(4\text{-}^i\text{BuC}_3\text{H}_4\text{N}_2)]$  (**7**), MMOH, RNR-R2, and  $\Delta 9\text{D}$ 

	$\delta$ (mm/s)	$\Delta E_Q$ (mm/s)	$\Gamma_L$ (mm/s)	$\Gamma_R$ (mm/s)	$J$ ( $\text{cm}^{-1}$ )	$g$	ref
<b>2</b>	1.26(2) <sup>a</sup>	2.90(2) <sup>a</sup>	0.27 <sup>a</sup>	0.28 <sup>a</sup>			<i>f</i>
<b>4</b>	1.19(2) <sup>a</sup>	3.02(2) <sup>a</sup>	0.25 <sup>a</sup>	0.25 <sup>a</sup>	-0.90(3) <sup>b</sup>	2.16(1)	<i>f</i>
<b>5</b>	1.19(2) <sup>a</sup>	3.01(2) <sup>a</sup>	0.34 <sup>a</sup>	0.40 <sup>a</sup>	-1.04(2) <sup>b</sup>	2.14(1)	<i>f</i>
<b>7</b>	1.12(2) <sup>a</sup>	3.05(2) <sup>a</sup>	0.24 <sup>a</sup>	0.26 <sup>a</sup>			<i>f</i>
MMOH	1.30 <sup>a,c</sup>	2.87 <sup>a,c</sup>					11
	1.3 <sup>a,d,e</sup>	2.4–3.1 <sup>a,d,e</sup>			0.3–0.5 <sup>b,d</sup>		51, 52
RNR-R2	1.26 <sup>a</sup>	3.13 <sup>a</sup>			-0.5 <sup>b</sup>		53, 54
$\Delta 9\text{D}$	1.30 <sup>a,e</sup>	3.04–3.36 <sup>a,e</sup>			$\sim -1$ <sup>b</sup>		9, 55

<sup>a</sup> Measured at 4.2 K. <sup>b</sup>  $\mathcal{H} = -2J\mathbf{S}_1 \cdot \mathbf{S}_2$ . <sup>c</sup> *Methylococcus capsulatus* (Bath). <sup>d</sup> *Methylosinus trichosporium* OB3b. <sup>e</sup> Two quadrupole doublets. <sup>f</sup> This work.

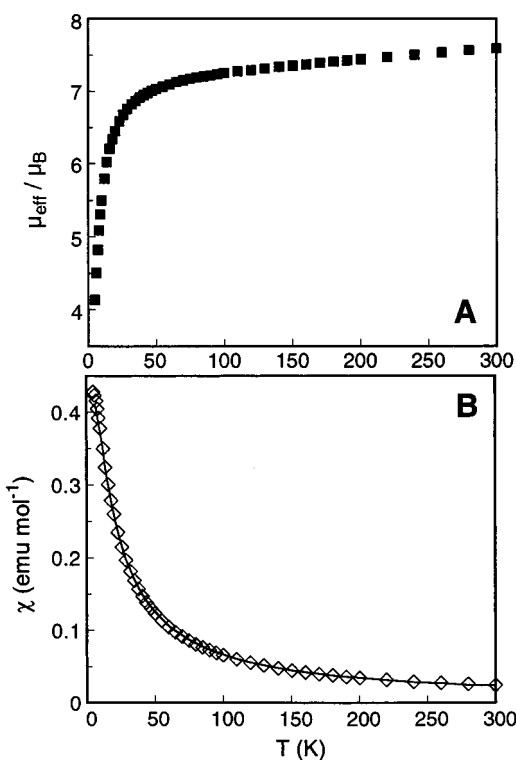


**Figure 5.** Plots of effective moment ( $\mu_{\text{eff}}$ ) per molecule versus temperature (A) and molar susceptibility ( $\chi_M$ ) versus temperature (B) for  $[\text{Fe}_2(\mu\text{-O}_2\text{CAr}^{\text{Tot}})_2(\text{O}_2\text{CAr}^{\text{Tot}})_2(\text{C}_5\text{H}_5\text{N})_2]$  (**4**). The solid line in B corresponds to the best fit, obtained by using the parameters described in Table 3.

displayed in Figure S13 (Supporting Information). The measured value of  $\mu_{\text{eff}} = 6.52 \mu_B$  at 300 K is substantially lower than those of **4** and **5**, in which there are two uncoupled  $S = 2$  centers. From 300 to 5 K, this value almost linearly decreases to  $0.42 \mu_B$  (Figure S13). Although this apparent strong AF coupling can be attributed to an increased number of bridging ligands as well as the shorter metal...metal distance in **7**, a satisfactory theoretical model to reproduce the magnetic behavior is currently unavailable.

**<sup>19</sup>F NMR Spectroscopic Studies.** The solution structures of **8** and **12** were probed by variable-temperature <sup>19</sup>F NMR spectroscopy. In  $\text{CH}_2\text{Cl}_2$  at 20 °C, **12** exhibits a sharp ( $\Delta\nu_{1/2} = 43$  Hz) resonance at -117.4 ppm (Figure S14, Supporting Information). This signal arises from the four  $\mu\text{-}1,3$   $\text{Ar}^{4\text{-FPh}}\text{CO}_2^-$  ligands, related by the pseudo- $C_4$  axis along the Fe–Fe vector. The local  $C_2$  symmetry of the  $\text{Ar}^{4\text{-FPh}}\text{CO}_2^-$  ligand apparently gives rise to a single fluorine resonance. The corresponding signal occurs at -115.5 ppm for dia-

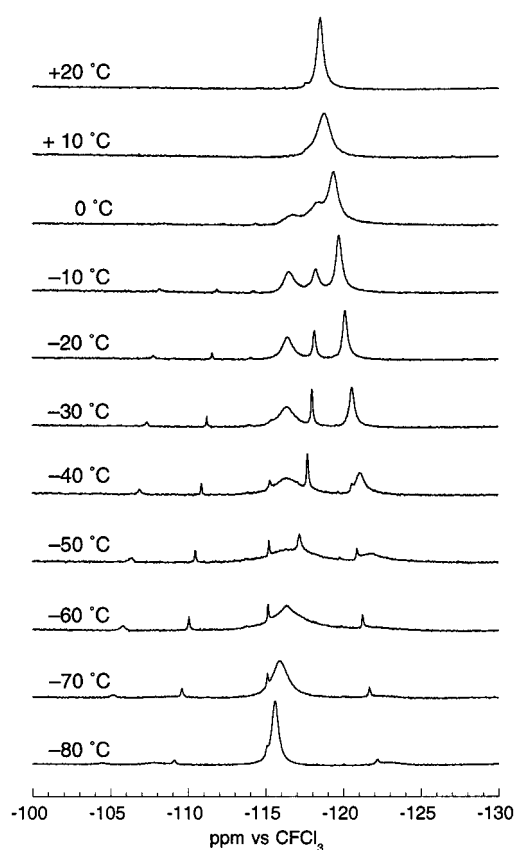


**Figure 6.** Variable-temperature <sup>19</sup>F NMR spectra (vs  $\text{CFCl}_3$ ) of  $[\text{Fe}_2(\mu\text{-O}_2\text{CAr}^{4\text{-FPh}})_2(\text{O}_2\text{CAr}^{4\text{-FPh}})_2(\text{THF})_2]$  (**8**) in  $\text{CH}_2\text{Cl}_2$  at 470 MHz.

magnetic  $\text{Ar}^{4\text{-FPh}}\text{CO}_2\text{H}$ , which shifts to -117.7 ppm upon deprotonation with excess  $\text{Et}_3\text{N}$  (data not shown). Within the temperature range of +20 to -70 °C, no significant spectral change was observed for **12** (Figure S14).

Under similar conditions, however, **8** displays much different spectral patterns (Figure 6). At 20 °C, a single broad ( $\Delta\nu_{1/2} = 213$  Hz) resonance occurs at -118.5 ppm, which significantly broadens ( $\Delta\nu_{1/2} = 438$  Hz) upon cooling to 10 °C. This signal splits into a set of three peaks between -120 and -116 ppm below 0 °C, with enhanced resolution at lower temperatures. At -20 °C, three well-resolved resonances occur at -120.1, -118.2, and -116.4 ppm. Notable spectral changes from -10 °C to -40 °C include sharpening of the peak at -118 ppm, along with significant broadening of the two flanking resonances at -120 and -116 ppm. These signals become barely resolved at -50 °C. The middle resonance at -118 ppm is slightly downfield shifted upon

cooling. Below  $-60\text{ }^{\circ}\text{C}$ , the three peaks merge into one broad resonance, which becomes narrower upon cooling. At  $-80\text{ }^{\circ}\text{C}$ , a single resonance at  $-115.6\text{ ppm}$  ( $\Delta\nu_{1/2} = 508\text{ Hz}$ ) dominates the  $^{19}\text{F}$  NMR spectrum of **8**. Along with this dramatic temperature-dependent spectral change, minor fluorine-containing species were also detected. Although their presence was obscured by overlap with the major signals at certain temperature ranges, four small peaks are persistent in the spectra obtained below  $-60\text{ }^{\circ}\text{C}$ . At  $-80\text{ }^{\circ}\text{C}$ , peaks at  $-104.4$ ,  $-109.1$ ,  $-115.1$ , and  $-122.1\text{ ppm}$  are observed in addition to the major resonance at  $-115.6\text{ ppm}$ .

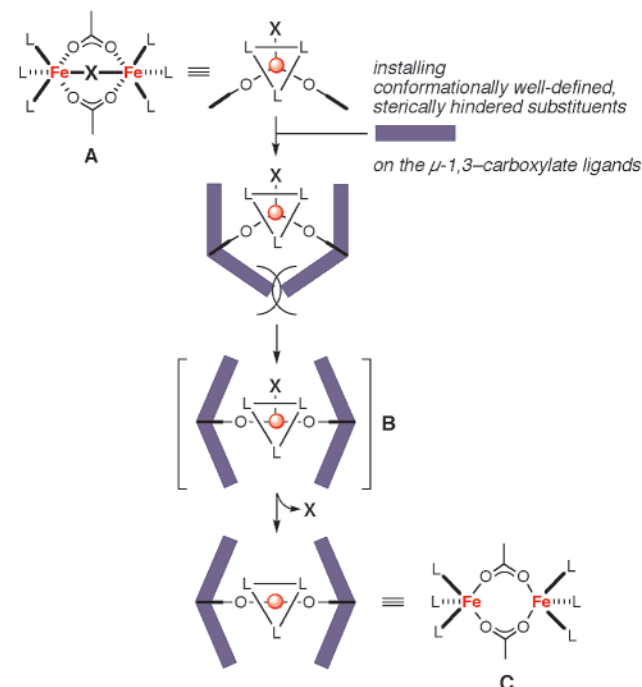
## Discussion

**Ligand Design.** The development of sterically demanding ligands has significantly advanced the chemistry of low-coordinate metal complexes.<sup>61,62</sup> Bulky *m*-terphenyl fragments have been previously used in main group organometallic chemistry to stabilize compounds having unusual structural or electronic properties.<sup>62–64</sup> Aryloxoide,<sup>65</sup> -thiolate,<sup>66</sup> -amidinate,<sup>67</sup> or -imide<sup>68</sup> derivatives having 2,6-aryl substituents stabilize coordinatively unsaturated metal sites.

In contrast to the widespread use of the *m*-terphenyl ligand fragments mentioned above, however, analogous platforms incorporating carboxylate functionalities have found limited applications in synthetic inorganic chemistry. Prior to our initial exploration of this area, there were only two structurally characterized transition metal complexes supported by *m*-terphenyl-derived carboxylate ligands. They are  $[\text{Rh}_2(\text{TTB})_3(\text{OAc})(\text{py})_2]$  and  $[\text{Rh}_2(\text{TTB})_4(\text{py})_2]$ , where TTB = 2,4,6-tri(*p*-tolyl)benzoate.<sup>69</sup> Related *m*-terphenyl-derived carboxylate units have been used to model host–guest interactions in organic chemistry.<sup>39c,70,71</sup>

Our investigation of diiron complexes coordinated by *m*-terphenyl-derived carboxylate ligands was inspired by the

**Scheme 3**



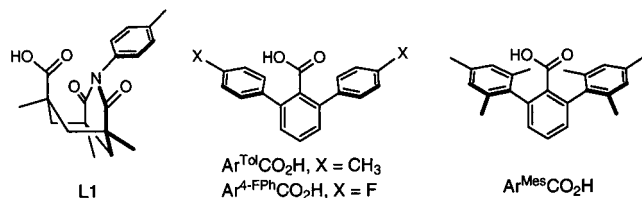
unusual spatial orientation of the two  $\mu$ -1,3 carboxylate groups supporting the diiron(II) centers in RNR-R2 and  $\Delta 9\text{D}$ .<sup>6,8</sup> A survey of the CSD revealed that a majority of structurally characterized carboxylate-bridged diiron complexes have triply bridged  $\{\text{Fe}_2(\mu\text{-O}_2\text{CR})_2(\mu\text{-X})\}^{n+}$  cores, where X = O, OH, or OR. Single-atom bridging ligands X in such dinuclear centers apparently enforce a geometry in which the two bridging carboxylate ligands occupy nearly orthogonal positions of face-shared octahedral metal centers (A, Scheme 3). We envisioned that, by increasing the steric repulsion between adjacent bridging carboxylate ligands, the  $\text{O}_{\text{carboxylate}}\text{-Fe-O}_{\text{carboxylate}}$  angle would open to such a degree that the triply bridged core geometry would be highly crowded (B, Scheme 3). Formal extrusion of the single-atom bridging ligand would afford the desired di( $\mu$ -carboxylato)diiron(II) cores in the resulting complexes (C, Scheme 3).

Unlike amine- or phosphine-based ligands, in which the immediate metal coordination can be controlled by direct substitution on the N- or P-donor atoms, modifications of a carboxylate ligand can only start from the carbon  $\alpha$  to the carboxylate group, three atoms away from the metal center. We reasoned that the desired trans configuration of two bridging carboxylate ligands would not be achieved simply by installing bulky substituents on the  $\alpha$ -carbons. Steric effects of the radially disposed bulky  $\alpha$ -substituents would propagate away from the metal center, significantly reducing the desired interligand steric repulsion. In order to maximize such steric crowding, bulky components on carboxylate ligands should be directed toward the dimetallic core.

In the quest for such a ligand system, we were attracted by the unique structural features of *m*-terphenyl-derived carboxylates. In these V-shaped molecules, aryl substituents flanking the  $\text{CO}_2^-$  group are directed toward the oxygen atoms and terminate nearly at their level. Although such

- (61) Cummins, C. C. *Prog. Inorg. Chem.* **1998**, *47*, 685–836.  
 (62) Twamley, B.; Haubrich, S. T.; Power, P. P. *Adv. Organomet. Chem.* **1999**, *44*, 1–65.  
 (63) (a) Robinson, G. H. *Acc. Chem. Res.* **1999**, *32*, 773–782. (b) Robinson, G. H. *Chem. Commun.* **2000**, 2175–2181.  
 (64) Clyburne, J. A. C.; McMullen, N. *Coord. Chem. Rev.* **2000**, *210*, 73–99.  
 (65) (a) O'Donoghue, M. B.; Schrock, R. R.; LaPointe, A. M.; Davis, W. M. *Organometallics* **1996**, *15*, 1334–1336. (b) Thorn, M. G.; Hill, J. E.; Waratuke, S. A.; Johnson, E. S.; Fanwick, P. E.; Rothwell, I. P. *J. Am. Chem. Soc.* **1997**, *119*, 8630–8641. (c) Thorn, M. G.; Etheridge, Z. C.; Fanwick, P. E.; Rothwell, I. P. *Organometallics* **1998**, *17*, 3636–3638. (d) Ooi, T.; Kondo, Y.; Maruoka, K. *Angew. Chem., Int. Ed.* **1998**, *37*, 3039–3041. (e) Vilardo, J. S.; Thorn, M. G.; Fanwick, P. E.; Rothwell, I. P. *Chem. Commun.* **1998**, 2425–2426. (f) Thorn, M. G.; Vilardo, J. S.; Fanwick, P. E.; Rothwell, I. P. *Chem. Commun.* **1998**, 2427–2428. (g) Darensbourg, D. J.; Niezgod, S. A.; Draper, J. D.; Reibenspies, J. H. *J. Am. Chem. Soc.* **1998**, *120*, 4690–4698.  
 (66) (a) Ellison, J. J.; Ruhlandt-Senge, K.; Power, P. P. *Angew. Chem., Int. Ed. Engl.* **1994**, *33*, 1178–1180. (b) Niemeyer, M.; Power, P. P. *Inorg. Chem.* **1996**, *35*, 7264–7272. (c) Buyuktas, B. S.; Olmstead, M. M.; Power, P. P. *Chem. Commun.* **1998**, 1689–1690. (d) Stange, A. F.; Sixt, T.; Kaim, W. *Chem. Commun.* **1998**, 469–470.  
 (67) Schmidt, J. A. R.; Arnold, J. *Chem. Commun.* **1999**, 2149–2150.  
 (68) Clark, G. R.; Nielson, A. J.; Rickard, C. E. *F. J. Chem. Soc., Dalton Trans.* **1996**, 4265–4268.  
 (69) Callot, H. J.; Albrecht-Gary, A.-M.; Joubbeh, M. A.; Metz, B. *Inorg. Chem.* **1989**, *28*, 3633–3640.  
 (70) Vinod, T. K.; Hart, H. In *Topics in Current Chemistry*; Weber, E., Ed.; Springer-Verlag: Berlin, 1994; Vol. 172, pp 119–178.  
 (71) Kannan, A.; Rajakumar, P.; Kabaleswaran, V.; Rajan, S. S. *J. Org. Chem.* **1996**, *61*, 5090–5102.

structural features are shared by the ligand L1,<sup>72</sup> previously employed to support ( $\mu$ -aqua)di( $\mu$ -carboxylato)dimetallic cores, steric shielding around the carboxylate group within the *m*-terphenyl unit is amplified by the pseudo- $C_2$  symmetry within the ligand. Preliminary CPK modeling studies suggested that 2,6-di(*p*-tolyl)benzoate ( $\text{Ar}^{\text{Tol}}\text{CO}_2^-$ ) would facilitate the assembly of the desired di( $\mu$ -carboxylato)diiron(II) cores. The requirement for the trans-disposed bridging carboxylate ligands in the  $\{\text{Fe}_2(\mu\text{-O}_2\text{CAR}^{\text{Tol}})_2\}^{2+}$  unit minimizes steric interactions between the *p*-tolyl groups. The related ligand 2,6-di(4-fluorophenyl)benzoate ( $\text{Ar}^{4\text{-FPh}}\text{CO}_2^-$ ) was also targeted in order to provide a handle for solution <sup>19</sup>F NMR spectroscopic studies.



The *m*-terphenyl unit is modular in nature, and variations can be readily made on the 2,6-substituents. Electronic perturbation introduced by such variations is substantially minimized since the conjugation between the central ring and the flanking substituents is conformationally prohibited. The C–C rotation responsible for such deconjugation of the aryl system, however, renders a certain degree of conformational flexibility to the terphenyl system, the importance of which can be highlighted by comparison with a more rigid 2,6-dimesitylbenzoate ( $\text{Ar}^{\text{Mes}}\text{CO}_2^-$ ) system used by others (vide infra).<sup>73</sup>

**Structural Models of  $\Delta$ 9D and RNR-R2 Active Sites.** Compounds **1–5** and **8** belong to a rare class of diiron(II) compounds in which two metal centers are bridged solely by two carboxylate ligands. This structural motif is encountered at diiron(II) centers in the active sites of reduced RNR-R2 and  $\Delta$ 9D,<sup>6,8</sup> as well as that in  $\text{MMOH}_{\text{red}}$ ,<sup>10</sup> and shared by a few structurally characterized complexes such as  $[\text{Fe}_2(\mu\text{-OAc})_2(\text{TPA})_2](\text{BPh}_4)_2$ ,<sup>24,74</sup>  $[\text{Fe}_2(\mu\text{-OAc})_2(\text{BPMEN})_2](\text{ClO}_4)_2$ ,<sup>24,75</sup> and  $[\text{Fe}_2(\mu\text{-O}_2\text{CPh})_2(\text{O}_2\text{CPh})_2(\text{C}_5\text{H}_5\text{N})_4]$ .<sup>76</sup> Although the doubly bridged dimetallic cores in these compounds are reminiscent of those in non-heme diiron enzyme active sites, neither the ligand type/composition nor the coordination geometry reproduces the properties of their biological counterparts. Polyamine/imine ancillary capping ligands render the metal coordinatively saturated

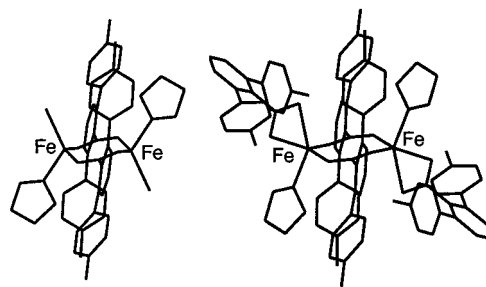


**Figure 7.** Structures of  $[\text{Fe}_2(\mu\text{-O}_2\text{CAR}^{\text{Tol}})_2(\text{THF})_2\text{Br}_2]$  (**1**) (left) and  $[\text{Fe}_2(\mu\text{-O}_2\text{CAR}^{\text{Tol}})_2(\text{O}_2\text{CAR}^{\text{Tol}})_2(\text{THF})_2]$  (**2**) (right), generated using the crystallographic coordinates.

with no open coordination sites available for exogenous ligand binding. This structural feature has a significant influence on the reactivity. For example,  $[\text{Fe}_2(\mu\text{-OAc})_2(\text{TPA})_2]^{2+}$  dissociates into two monomeric units in order to react with dioxygen.<sup>74</sup> Di( $\mu$ -carboxylato)diiron(II) complexes having coordinatively unsaturated metal centers were previously unknown in synthetic inorganic chemistry.

The diiron(II) core structure of **4** bears a close structural resemblance to the catalytic site of  $\Delta$ 9D (Figures 1, 2, and S15 (Supporting Information)). The two  $\mu$ -1,3-bridging carboxylate ligands of the model simulate the Glu143 and Glu229 residues, which span two iron(II) centers in the protein. Bidentate binding of Glu105 and Glu196, as well as the coordination of two nitrogen donors, His146 and His232, is reproduced by the terminal carboxylate and pyridine ligands. The  $\text{Fe}\cdots\text{Fe}$  separation of 4.2189(13) Å in **4** models the corresponding value of 4.2 Å in  $\Delta$ 9D.<sup>8</sup> This relatively long metal $\cdots$ metal distance results from steric interactions between bridging and terminal carboxylate ligands, as clearly indicated by the solid state structures of the related compounds **1** and **2** (Figure 7). Here the identical  $\{\text{Fe}_2(\mu\text{-O}_2\text{CAR}^{\text{Tol}})_2(\text{THF})_2\}^{2+}$  cores are capped either by  $\text{Br}^-$  (**1**) or by a bidentate  $\text{Ar}^{\text{Tol}}\text{CO}_2^-$  (**2**) ligand. Steric repulsion between the *p*-tolyl groups on the bridging and terminal carboxylate ligands apparently pushes the two iron atoms away from each other, increasing the  $\text{Fe}\cdots\text{Fe}$  distance by as much as ca. 0.7 Å, from 3.568(1) Å in **1** to 4.2822(7) Å in **2**. The geometry of the first coordination sphere thus can be tuned by noncovalent interaction in the second coordination sphere, which comprises four interlocking *m*-terphenyl units. Although the diiron core in **4** is effectively shielded by these sterically hindered ligands, the open coordination site of the five-coordinate iron atom is well-exposed (Figure 3) for reaction with exogenous reagents including dioxygen.<sup>32,35</sup>

Features of the doubly bridged four-coordinate diiron(II) centers in the active site of RNR-R2 are mimicked by **5** (Figures 1, 2, and S16 (Supporting Information)).<sup>6</sup> The coordination of  $\mu$ -1,3 bridging Glu115 and Glu238, terminal monodentate Asp84 and Glu204, and N-donor His118 and His241 residues in the protein is faithfully represented by the diiron(II) core in 4,4-coordinate **5**. The  $\text{Fe}\cdots\text{Fe}$  separation of 4.2029(10) Å is similar to that (3.9 Å) in the protein. The Mössbauer and magnetic parameters of **4** and **5** are comparable to the corresponding properties of  $\Delta$ 9D and RNR-R2,

(72) Hagen, K. S.; Lachicotte, R.; Kitaygorodskiy, A. *J. Am. Chem. Soc.* **1993**, *115*, 12617–12618.

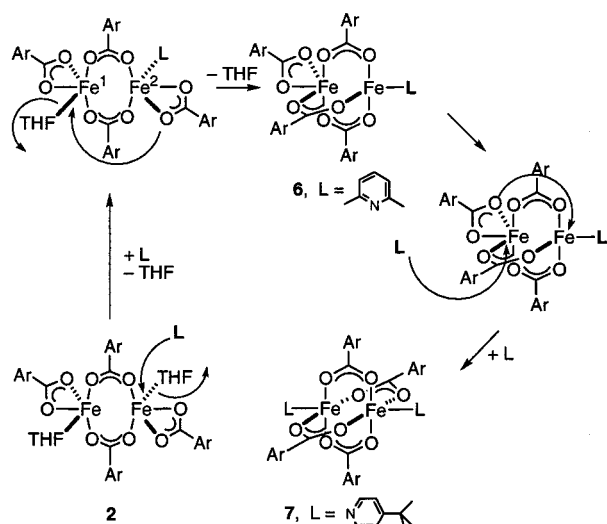
(73) (a) Hagadorn, J. R.; Que, L., Jr.; Tolman, W. B. *J. Am. Chem. Soc.* **1998**, *120*, 13531–13532. (b) Hagadorn, J. R.; Que, L., Jr.; Tolman, W. B.; Prisca, I.; Münck, E. *J. Am. Chem. Soc.* **1999**, *121*, 9760–9761. (c) Hagadorn, J. R.; Que, L., Jr.; Tolman, W. B. *Inorg. Chem.* **2000**, *39*, 6086–6090.

(74) Ménage, S.; Zang, Y.; Hendrich, M. P.; Que, L., Jr. *J. Am. Chem. Soc.* **1992**, *114*, 7786–7792.

(75) Hazell, R.; Jensen, K. B.; McKenzie, C. J.; Toftlund, H. *J. Chem. Soc., Dalton Trans.* **1995**, 707–717.

(76) Randall, C. R.; Shu, L.; Chiou, Y.-M.; Hagen, K. S.; Ito, M.; Kitajima, N.; Lachicotte, R. J.; Zang, Y.; Que, L., Jr. *Inorg. Chem.* **1995**, *34*, 1036–1039.

Scheme 4



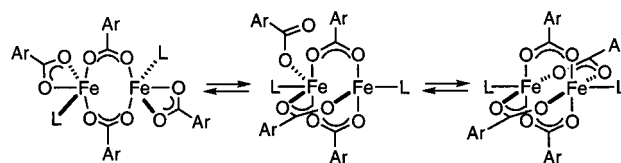
for which weak AF coupling between high-spin iron(II) centers affords a  $S = 0$  ground state (Table 3).

Although **4** and **5** faithfully reproduce the ligand composition and coordination number of the diiron(II) active sites of  $\Delta 9D$  and RNR-R2, certain limitations exist. The relative positioning of the N-donor ligands is different. They are disposed anti in the model compound (Figure 2) and syn in the protein (Figure 1). If such an asymmetric ligand arrangement is crucial in order to bind substrates in the right orientation, the symmetry-related iron sites in **4** or **5** may not be ideal for the desired biomimetic chemical transformations. Spatial disposition of the ancillary ligands can have a significant influence on chemical reactivity by affecting the structures and energies of the molecular orbitals involved. These stereoelectronic issues remain to be addressed by future work.

**Ligand Substitution and Core Rearrangement.** Depending on the choice of N-donor ligands, doubly, triply, or quadruply bridged diiron(II) cores can be accessed (Schemes 1 and 2). Reaction of **2** with MeCN, pyridine, or 1-methylimidazole introduces minimal structural perturbation at the metal centers. The  $\{\text{Fe}_2(\mu\text{-O}_2\text{CAR}^{\text{Tot}})_2(\text{O}_2\text{CAR}^{\text{Tot}})_2\}$  core structure is retained. Shifts of one or two carboxylate ligands occur, however, upon ligand substitution of **2** with 2,6-lutidine or 4-*tert*-butylpyridine. One possible mechanism for such core conversions is postulated in Scheme 4. Formal shift of one carboxylate from terminal bidentate to  $\mu$ -1,3-bridging is triggered by displacing the THF ligand in **2** with 2,6-lutidine. The two  $\alpha$ -methyl groups of 2,6-lutidine induce steric crowding around the Fe–N bond, lowering the coordination number of Fe(2) from five to four. Such a carboxylate shift would displace the THF ligand on Fe(1) and afford the asymmetric 4,5-coordination encountered in **6**.

Formal double carboxylate shifts within the  $\{\text{Fe}_2(\mu\text{-O}_2\text{CAR}^{\text{Tot}})_2(\text{O}_2\text{CAR}^{\text{Tot}})_2\}$  unit triggered by ligand substitution would afford the paddlewheel complex **7** (Scheme 4). The 4-*tert*-butylpyridine ligand was initially employed to enhance the solubility of **4**, which hampered solution spectroscopic studies. The bulky 4-*tert*-butyl group was installed distal to

Scheme 5



the N-donor atom, in order to minimize structural perturbation. A space-filling model indicated little steric crowding in the desired compound  $[\text{Fe}_2(\mu\text{-O}_2\text{CAR}^{\text{Tot}})_2(\mu\text{-O}_2\text{CAR}^{\text{Tot}})_2]^{2-}$  (4-*t*-BuC<sub>5</sub>H<sub>4</sub>N)<sub>2</sub>). The quadruply bridged diiron(II) core in **7**, therefore, was not anticipated before its structural characterization by X-ray crystallography. Although two metal ions bridged by four carboxylate ligands define a well-known unit in inorganic chemistry, **7** is only the third structurally characterized example in iron(II) chemistry. The others are  $[\text{Fe}_2(\mu\text{-O}_2\text{CCMe}_3)_4(\text{C}_5\text{H}_5\text{N})_2]$  and  $[\text{Fe}_2(\mu\text{-O}_2\text{CPh})_4(\text{C}_5\text{H}_5\text{N})_2]$ .<sup>76</sup> A gradual decrease in metal...metal distance with additional bridging ligands places the Fe...Fe distance of 2.8229(9) Å in **7** at the low end of the range obtained for the Ar<sup>Tot</sup>CO<sub>2</sub><sup>-</sup>-based tetracarboxylate diiron(II) complexes (Tables 1 and 2). Comparable metal...metal distances of 2.792 and 2.851 Å were obtained for  $[\text{Fe}_2(\mu\text{-O}_2\text{CCMe}_3)_4(\text{C}_5\text{H}_5\text{N})_2]$  and  $[\text{Fe}_2(\mu\text{-O}_2\text{CPh})_4(\text{C}_5\text{H}_5\text{N})_2]$ , respectively.<sup>77</sup>

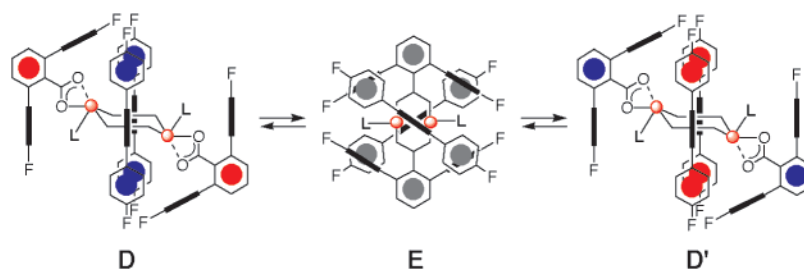
**Doubly vs Quadruply Bridged Tetracarboxylate Diiron(II) Complexes.** Two geometric isomers,  $[\text{Fe}_2(\mu\text{-O}_2\text{CAR}^{4\text{-FPh}})_2(\text{O}_2\text{CAR}^{4\text{-FPh}})_2(\text{THF})_2]$  (**8**) and  $[\text{Fe}_2(\mu\text{-O}_2\text{CAR}^{4\text{-FPh}})_4(\text{THF})_2]$  (**9**), were obtained for  $[\text{Fe}_2(\text{O}_2\text{CAR}^{4\text{-FPh}})_4(\text{THF})_2]$ . Isolation and structural characterization of **8** and **9** strongly indicate that both windmill and paddlewheel diiron(II) cores can be accessed without substantial steric or electronic preference under the conditions employed.

The substitution reactions of **8** with N-donor ligands afford only quadruply bridged diiron(II) complexes (**10–12**), whereas both doubly and quadruply bridged complexes are accessible by similar synthetic routes from **2**. As evident from Schemes 1 and 2, no obvious correlation can be drawn between the preferred solid state structures and the steric/electronic properties of the ancillary ligands within a homologous series. For example, both pyridine and 4-*tert*-butylpyridine afford tetra( $\mu$ -carboxylato)diiron(II) cores supported by Ar<sup>4-FPh</sup>CO<sub>2</sub><sup>-</sup>, whereas they provide doubly and quadruply bridged diiron(II) complexes, respectively, for the Ar<sup>Tot</sup>CO<sub>2</sub><sup>-</sup> system. Although the ability to acquire X-ray crystal structures of these complexes assured their structural homogeneity in the solid state, there is no clear answer as to why a given complex prefers one isomer over the other and how both isomers can be accessed for a certain ligand combination.

These findings led us to speculate that at least two isomeric forms exist for  $[\text{Fe}_2(\mu\text{-O}_2\text{CAR}')_4\text{L}_2]$  complexes in solution, the interconversion between which is assisted by carboxylate shifts (Scheme 5). Equilibration among these species can be affected by various factors including solvent polarity and temperature. At the early stage of crystallization, a weak packing interaction may lead to selective deposition of one

(77) Hagen, K. S. Personal communication.

Scheme 6



isomer, and the thermodynamically driven crystallization process can afford structural homogeneity in the solid state. In order to probe the possibility that such dynamic structural rearrangements occur within the tetracarboxylate diiron(II) platform, solution NMR studies were carried out.

**Structural Rearrangement Probed by Variable-Temperature  $^{19}\text{F}$  NMR Spectroscopy.** The presence of fluorine nuclei in the  $\text{Ar}^{4-\text{FPh}}\text{CO}_2^-$  ligands allowed the use of  $^{19}\text{F}$  NMR spectroscopy to investigate the solution structures of **8** and **12**, despite their paramagnetism.  $^{19}\text{F}$  NMR spectroscopy is a good structural probe for paramagnetic iron(II) or cobalt(II) complexes.<sup>72,78–80</sup> The number and symmetry of the species in solution can often be inferred from the spectral pattern, which is significantly simplified compared with that of  $^1\text{H}$  NMR.

Unlike the large isotropic shifts ( $\Delta\text{ppm} > \sim 55$ ) of iron(II)-bound  $\text{CF}_3\text{CO}_2^-$  or  $\text{OTf}^-$ ,<sup>78,80</sup> coordinated  $\text{Ar}^{4-\text{FPh}}\text{CO}_2^-$  ligands in **8** and **12** display resonances ( $-118.5$  to  $-117.4$  ppm) only slightly shifted from that ( $-117.7$  ppm) of the diamagnetic free  $\text{Ar}^{4-\text{FPh}}\text{CO}_2^-$  anion at  $20^\circ\text{C}$ . This narrow range of chemical shifts may result from the relatively long  $\text{F}\cdots\text{Fe}$  distances of  $> \sim 5.87$  Å in **8** and  $> \sim 5.62$  Å in **12**, as well as by the absence of efficient spin delocalization pathways. Nevertheless, the temperature-dependent changes in the  $^{19}\text{F}$  NMR spectral patterns are markedly different for **8** and **12**, allowing us to draw conclusions about the solution behavior.

Consistent with the pseudo- $C_4$  symmetry found for the paddlewheel structure of **12** in the solid state, a single fluorine resonance was observed at  $20^\circ\text{C}$ . Combined with the local pseudo- $C_2$  symmetry of the  $\text{Ar}^{4-\text{FPh}}\text{CO}_2^-$  ligand, the disposition of the four ligand fragments along the  $\text{Fe}-\text{Fe}$  vector places the eight fluorine nuclei at the corners of an approximately rectangular parallelepiped. The  $\text{F}\cdots\text{Fe}$  distances are distributed over a narrow range of  $5.62-6.22$  Å in the solid state, and the fluorine atoms experience similar local magnetic environments. This simple spectral pattern is displayed from  $+20$  to  $-70^\circ\text{C}$ , suggesting that the quadruply bridged core structure of **12** is retained in  $\text{CH}_2\text{Cl}_2$  over this temperature range.

A significantly broadened ( $\Delta\nu_{1/2} = 213$  Hz) fluorine resonance of **8**, compared with that ( $\Delta\nu_{1/2} = 43$  Hz) of **12**,

at  $20^\circ\text{C}$  indicates either rapid equilibration between multiple  $\text{Ar}^{4-\text{FPh}}\text{CO}_2^-$ -containing species or different chemical environments for the fluorine nuclei of a single species. Either explanation can be invoked in order to explain the dramatic spectral change of **8** from  $+20$  to  $-80^\circ\text{C}$  (Figure 6). As depicted in Scheme 6, we postulate an equilibration between doubly bridged (**D** and **D'**) and quadruply bridged (**E**) isomers of  $[\text{Fe}_2(\text{O}_2\text{CAR}^{4-\text{FPh}})_4(\text{THF})_2]$  in  $\text{CH}_2\text{Cl}_2$  at  $20^\circ\text{C}$ . This assignment is strongly supported by the isolation of **8** and **9** (vide supra) at room temperature ( $\sim 25^\circ\text{C}$ ). The individual fluorine signals arising from such an equilibrium mixture are unresolved above  $+10^\circ\text{C}$ , which we ascribe to dynamic interconversion between isomers. Three distinct peaks emerge below  $0^\circ\text{C}$ . Such a pattern could be accounted for by the  $\mu$ -1,3-bridging and terminal  $\text{Ar}^{4-\text{FPh}}\text{CO}_2^-$  ligands in **D**, which are rendered inequivalent due to their different chemical environments (Scheme 6). Alternatively, the sharp peak in the middle of the three signals can be assigned to **E**, by analogy to the narrow fluorine resonance observed for **12** under similar conditions. With the latter model, the two broader flanking signals are assigned to the  $\mu$ -1,3-bridging and terminal carboxylate ligands in **D**. The  $^1\text{H}$  NMR spectrum obtained for the diamagnetic compound  $[\text{Zn}_2(\mu\text{-O}_2\text{CAR}^{\text{Tot}})_2(\text{O}_2\text{CAR}^{\text{Tot}})_2(\text{C}_5\text{H}_5\text{N})_2]$ , which is structurally related to **D**, displays two different methyl resonances at 2.07 and 2.02 ppm in  $\text{CH}_2\text{Cl}_2$  at  $20^\circ\text{C}$ .<sup>81</sup> This behavior is consistent with the different magnetic environments of the *p*-tolyl groups on the bridging and terminal  $\text{Ar}^{\text{Tot}}\text{CO}_2^-$  ligands. A mixture of **D/D'** and **E** would result in the three major fluorine resonances observed experimentally.

At lower temperatures, the exchange rate of the carboxylate ligands in **D** between the bridging and terminal positions slows down, as reflected by significant broadening of the signals at  $-116$  and  $-120$  ppm, which merge into the resonance arising from **E**. Below  $-60^\circ\text{C}$ , **D** eventually converts to **E** and a single fluorine signal from its equivalent  $\text{Ar}^{4-\text{FPh}}\text{CO}_2^-$  groups dominates the spectra. The four well-resolved small peaks between  $-104$  and  $-122$  ppm, partially overlapping the major fluorine resonances, may arise from other  $\text{Ar}^{4-\text{FPh}}\text{CO}_2^-$ -containing species. One possibility would be a triply bridged diiron(II) species structurally related to the  $\text{Ar}^{\text{Tot}}\text{CO}_2^-$ -supported complex **6**, in which all four fluorine resonances are inequivalent.

Although a more definitive proof of the foregoing core rearrangement mechanism is currently unavailable, the dynamic nature of the carboxylate ligands within the tetra-

(78) Hagen, K. S.; Lachicotte, R.; Kitaygorodskiy, A.; Elbouadili, A. *Angew. Chem., Int. Ed. Engl.* **1993**, *32*, 1321–1324.

(79) Lachicotte, R.; Kitaygorodskiy, A.; Hagen, K. S. *J. Am. Chem. Soc.* **1993**, *115*, 8883–8884.

(80) Blakesley, D. W.; Payne, S. C.; Hagen, K. S. *Inorg. Chem.* **2000**, *39*, 1979–1989.

(81) Lee, D.; Lippard, S. J. Unpublished result.

carboxylate diiron framework is clearly demonstrated. Similar processes can be operative within a related construct. Previous Mössbauer studies of  $[\text{Fe}_2(\mu\text{-BXDK})(\mu\text{-O}_2\text{CPhCy})(\text{O}_2\text{CPhCy})(\text{C}_5\text{H}_5\text{N})_2]$  revealed that its solid and solution structures may not be the same.<sup>28</sup> In the solid state, this compound consists of one six-coordinate and one four-coordinate iron atom, which afford two distinct quadrupole doublets. The Mössbauer spectrum obtained for a frozen THF solution sample, however, displays a single broad quadrupole doublet. This spectral behavior may arise from scrambling between the  $\mu$ -1,3-bridging and terminal bidentate carboxylate ligand in solution, which would render the two iron sites equivalent.

Carboxylate shifts within a diiron(II) core have a significant mechanistic implication for its reaction with dioxygen. Positioning of the open coordination sites for exogenous ligands can be adjusted by the ancillary ligands. For a molecule in which such structural variation is temperature-dependent, the functionally reactive isomer may be accessed under conditions mapped out by solution spectroscopic studies. Spectroscopic data obtained on frozen solutions of samples reflect the static structural properties of the molecules at the freezing point of the solution, which may not be the functionally relevant temperature.

**Flexibility versus Rigidity.** A sterically more demanding *m*-terphenyl-derived carboxylate ligand, 2,6-dimesitylbenzoate ( $\text{Ar}^{\text{Mes}}\text{CO}_2^-$ ), was used by others to assemble a related diiron(II) complex  $[\text{Fe}_2(\mu\text{-O}_2\text{CAr}^{\text{Mes}})_2(\text{O}_2\text{CAr}^{\text{Mes}})_2(\text{MeCN})_2]$ .<sup>73a</sup> The relatively long  $\text{Fe}\cdots\text{Fe}$  distance of 4.122(1) Å, as well as the composition of two  $\mu$ -1,3-bridging and two terminal bidentate carboxylate ligands, in this compound is reminiscent of the structural features of **2–5** and **8**. Coordination of this more sterically crowded ligand, however, affords a geometry that is significantly more rigid than that imposed by the less sterically demanding  $\text{Ar}^{\text{Tol}}\text{CO}_2^-$ , although the lateral width spanned by both compounds is identical. The presence of four ortho methyl groups in the biphenyl units of  $\text{Ar}^{\text{Mes}}\text{CO}_2^-$  apparently restricts rotation around the C–C bonds and enhances interligand steric repulsions. This behavior is clearly evident by a comparison of the  $[\text{Fe}_2(\mu\text{-O}_2\text{CAr}^{\text{Mes}})_2(\text{O}_2\text{CAr}^{\text{Mes}})_2(\text{MeCN})_2]$  and  $[\text{Fe}_2(\mu\text{-O}_2\text{CAr}^{\text{Tol}})_2(\text{O}_2\text{CAr}^{\text{Tol}})_2(\text{MeCN})_2]$  (**3**) structures. As displayed in Figure 8, in order to minimize steric interactions with the bridging carboxylate ligands, the terminal carboxylates in  $[\text{Fe}_2(\mu\text{-O}_2\text{CAr}^{\text{Mes}})_2(\text{O}_2\text{CAr}^{\text{Mes}})_2(\text{MeCN})_2]$  approach the iron atoms along the Fe–Fe vector, the  $\text{Fe}\cdots\text{Fe}\cdots\text{C}_{\text{carboxylate}}$  angle being 177.5°. Such mutual orthogonality of the four  $\text{Ar}^{\text{Mes}}\text{CO}_2^-$  fragments alleviates steric crowding between the conformationally more demanding ligands. Such a spatial disposition of ligands effectively shields the dimetallic core from external nucleophiles, and only the small rod-shaped MeCN ligand could be accommodated in the sterically crowded intermetallic cavity. Notably, the methyl group of the MeCN ligand is directing *toward* the diiron core. Attempts to install other N-donor ligands on the  $\{\text{Fe}_2(\mu\text{-O}_2\text{CAr}^{\text{Mes}})_2(\text{O}_2\text{CAr}^{\text{Mes}})_2\}$  platform resulted in core disassembly, affording mononuclear species.<sup>73a,c</sup>

Unlike the situation in  $[\text{Fe}_2(\mu\text{-O}_2\text{CAr}^{\text{Mes}})_2(\text{O}_2\text{CAr}^{\text{Mes}})_2(\text{MeCN})_2]$ , positioning of the two terminal bidentate  $\text{Ar}^{\text{Tol}}\text{CO}_2^-$

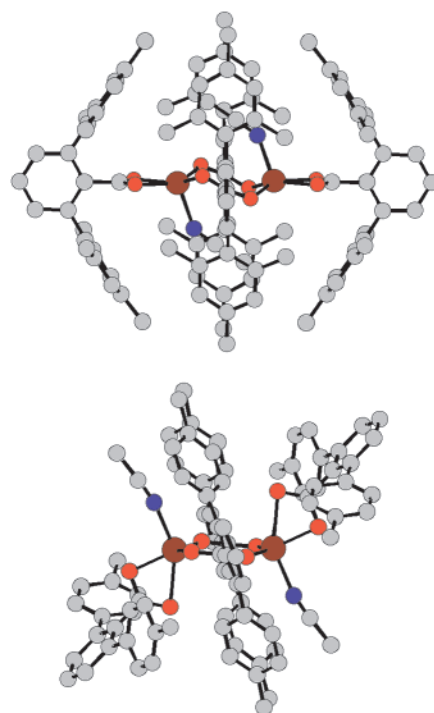


**Figure 8.** Structures of  $[\text{Fe}_2(\mu\text{-O}_2\text{CAr}^{\text{Mes}})_2(\text{O}_2\text{CAr}^{\text{Mes}})_2(\text{MeCN})_2]$  (top) and  $[\text{Fe}_2(\mu\text{-O}_2\text{CAr}^{\text{Tol}})_2(\text{O}_2\text{CAr}^{\text{Tol}})_2(\text{MeCN})_2]$  (**3**) (bottom), generated using the crystallographic coordinates.

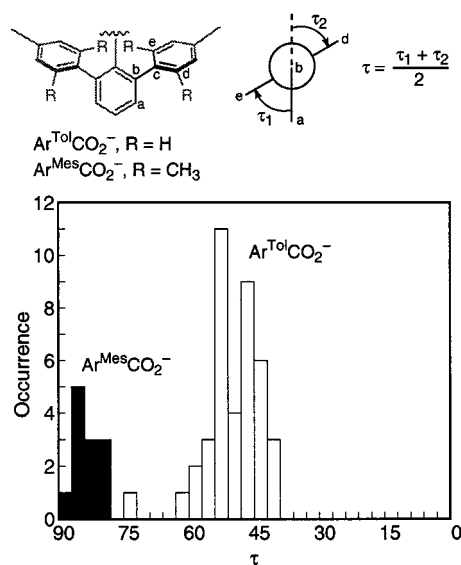


**Figure 9.** Distribution of torsion angles ( $\tau$ ) of  $\text{Ar}^{\text{Mes}}\text{CO}_2^-$  (■) and  $\text{Ar}^{\text{Tol}}\text{CO}_2^-$  (□) defined as  $(\tau_1 + \tau_2)/2$ . The values for  $\text{Ar}^{\text{Mes}}\text{CO}_2^-$  were obtained from CSD files BAWYUT, BAWZAA, and BAXBIL, corresponding to  $[\text{Li}_2(\mu\text{-O}_2\text{CAr}^{\text{Mes}})_2(\text{Et}_2\text{O})_2]$ ,  $[\text{Fe}(\text{O}_2\text{CAr}^{\text{Mes}})_2(1\text{-MeIm})_2]$ , and  $[\text{Fe}_2(\mu\text{-O}_2\text{CAr}^{\text{Mes}})_2(\text{O}_2\text{CAr}^{\text{Mes}})_2(\text{MeCN})_2]$ , respectively. Those of  $\text{Ar}^{\text{Tol}}\text{CO}_2^-$  were from **1–8**.

ligands in **3** significantly displaces them from the Fe–Fe vector, with an  $\text{Fe}\cdots\text{Fe}\cdots\text{C}_{\text{carboxylate}}$  angle of 125.5° (Figure 8). Rotation about the C–C bonds within the  $\text{Ar}^{\text{Tol}}\text{CO}_2^-$  ligand apparently reduces the steric repulsion, as the terminal carboxylates tilt toward the bridging carboxylates to open up a binding site for MeCN. Coordination of the MeCN ligand directs the methyl group *away from* the dimetallic core, and bulkier N-donor ligands can occupy this position without interligand steric repulsion. The  $\{\text{Fe}_2(\mu\text{-$

$\text{O}_2\text{CAr}^{\text{Tol}}_2(\text{O}_2\text{CAr}^{\text{Tol}})_2\}$  module retains its structural integrity upon coordination of biomimetic N-donor ligands, allowing the formation of a variety of diiron(II) complexes that are apparently inaccessible to the  $\text{Ar}^{\text{Mes}}\text{CO}_2^-$  system.

The ability to compare solid state structures of both  $\text{Ar}^{\text{Tol}}\text{CO}_2^-$ - and  $\text{Ar}^{\text{Mes}}\text{CO}_2^-$ -supported diiron(II) complexes enabled us to assess the flexibility of the ligand system as measured by the dihedral angle ( $\tau$ ) defined in Figure 9. Since the four carbon atoms  $\text{C}_b$ ,  $\text{C}_c$ ,  $\text{C}_d$ , and  $\text{C}_e$  may not lie in the same plane, an average value ( $\tau$ ) of the two angles ( $\tau_1$  and  $\tau_2$ ) was taken. Depending on the relative orientation of the two aryl rings, this value can range from  $90^\circ$  (orthogonal) to  $0^\circ$  (coplanar). The torsional confinement in  $\text{Ar}^{\text{Mes}}\text{CO}_2^-$  is reflected by the narrow range of  $\tau$  values, between  $80^\circ$  and  $87^\circ$ . For  $\text{Ar}^{\text{Tol}}\text{CO}_2^-$ , this value is distributed between  $40^\circ$  and  $74^\circ$ , indicating a significantly greater degree of freedom in aryl–aryl rotations. Such rotational flexibility within a conformationally rigid framework clearly distinguishes  $\text{Ar}^{\text{Tol}}\text{CO}_2^-$  from  $\text{Ar}^{\text{Mes}}\text{CO}_2^-$ , the consequence of which is reflected in distinctive structural and reactivity properties of the diiron complexes supported thereupon.<sup>32–35,73,82</sup>

## Conclusions

A general synthetic strategy is described that allows access to carboxylate-bridged diiron(II) complexes having unprecedented coordination geometries. Sterically demanding *m*-terphenyl-derived carboxylate ligands stabilize coordinatively unsaturated diiron(II) centers and faithfully reproduce key architectural aspects of the catalytic sites of selected non-heme diiron enzyme. With different carboxylate and N-donor

ligand (L) combinations in  $[\text{Fe}_2(\text{O}_2\text{CAr}^{\text{Tol}})_4\text{L}_2]$  complexes, both paddlewheel and windmill structures are encountered in the solid state structures. Carboxylate shifts, such as those encountered in the enzymes,<sup>1,10b,36</sup> accompany these structural changes. The structural flexibility within the carboxylate-rich ligand framework in solution was further demonstrated by variable-temperature  $^{19}\text{F}$  NMR spectroscopic studies. Temperature-dependent core interconversions are identified that facilitate attack by an incoming dioxygen molecule at an open coordination site for binding and activation. These processes are important for interpreting the results of the dioxygen reactivity of the  $[\text{Fe}_2(\text{O}_2\text{CAr}^{\text{Tol}})_4\text{L}_2]$  complexes, as discussed elsewhere.<sup>35</sup>

**Acknowledgment.** This work was supported by grants from the National Science Foundation and National Institute of General Medical Sciences. D.L. was the recipient of a Corning Foundation Science Fellowship in chemistry. We thank Ms. J. Kuzelka for help in acquiring the Mössbauer spectra, Drs. T. J. Mizoguchi and J. Du Bois for helpful discussions, and Prof. K. S. Hagen for providing the X-ray coordinates of the compounds  $[\text{Fe}_2(\mu\text{-O}_2\text{CCMe}_3)_4(\text{C}_5\text{H}_5\text{N})_2]$  and  $[\text{Fe}_2(\mu\text{-O}_2\text{CPh})_4(\text{C}_5\text{H}_5\text{N})_2]$ .

**Supporting Information Available:** Crystallographic information on **1–12** (Table S1). Figures S1–S10 showing ORTEP diagrams of **1**, **3**,  $[\text{FeTi}(\mu\text{-O}_2\text{CAr}^{\text{Tol}})_3(\text{C}_5\text{H}_5\text{N})]$ ,  $[\text{FeTi}(\mu\text{-O}_2\text{CAr}^{\text{Tol}})_3(1\text{-MeIm})]$ , **6**, and **8–12**. Physical characterization of **2**, **5**, **7**, and **12** (Figures S11–S14), solid state structure of **4** and **5** (Figures S15 and S16), and an X-ray crystallographic file (CIF). This material is available free of charge via the Internet at <http://pubs.acs.org>.

IC020186Y

(82) Lee, D.; Krebs, C.; Huynh, B. H.; Hendrich, M. P.; Lippard, S. J. *J. Am. Chem. Soc.* **2000**, *122*, 5000–5001.